Journal of
Marine Science and Engineering

MDPI

Article

A Two-Stage Optimisation of Ship Hull Structure Combining Fractional Factorial Design Technique and NSGA-II Algorithm

Joynal Abedin [1], Francis Franklin [1] and S. M. Ikhtiar Mahmud [2,*]

[1] School of Engineering, Newcastle University, Newcastle upon Tyne NE1 7RU, UK; j.abedin2@newcastle.ac.uk (J.A.); francis.franklin@newcastle.ac.uk (F.F.)
[2] Department of Naval Architecture and Marine Engineering, Military Institute of Science and Technology, Mirpur Cantonment, Dhaka 1216, Bangladesh
* Correspondence: ikhtiar@name.mist.ac.bd

Abstract: The intricate nature of ships and floating structures presents a significant challenge for ship designers when determining suitable structural dimensions for maritime applications. This study addresses a critical research gap by focusing on a three-cargo hold model for a multipurpose cargo ship. The complex composition of these structures, including stiffening plates, deck plates, bottom plates, frames, and bulkheads, necessitates thorough structural analysis to facilitate effective and cost-efficient design evaluation. To address this challenge, the research utilises FEMAP-integrated NX NASTRAN software (2021.2) to assess hull girder stress. Furthermore, a novel approach is introduced, integrating the Design of Experiments (DOE) principles within Minitab 21.4.1 software to identify critical parameters affecting hull girder stress and production costs. This method determined the top five key parameters influencing hull girder stress: Hatch coaming plate, Hatch coaming top plate, Main deck plate, Shear strake plate, and Bottom plate, while also highlighting key parameters that impact production costs: the inner bottom plate, Inner side shell plate, Bottom plate, Web frame spacing, and Side shell plate. Ship design optimisation is then carried out by incorporating regression equations from Minitab software into the Non-dominated Sorting Genetic Algorithm II (NSGA-II), which is managed using Python software (PyCharm Community Editon 2020.3.1). This optimisation process yields a significant 10% reduction in both ship weight and production costs compared to the previous design, achieved through prudent adjustments in plate thickness, web frame positioning, and stiffener arrangement. The optimally designed midship section undergoes rigorous validation to ensure conformity with industry standards and classification society regulations. Necessary adjustments to inner bottom plates and double bottom side girders are made to meet these stringent requirements. This research offers a comprehensive framework for the structural optimisation of ship hulls, potentially enhancing safety, sustainability, and competitiveness within the maritime engineering industry.

Keywords: scantlings; structural analysis; optimisation; DOE; fractional factorial design

Citation: Abedin, J.; Franklin, F.; Mahmud, S.M.I. A Two-Stage Optimisation of Ship Hull Structure Combining Fractional Factorial Design Technique and NSGA-II Algorithm. *J. Mar. Sci. Eng.* **2024**, *12*, 411. https://doi.org/10.3390/jmse12030411

Academic Editor: George Zaraphonitis

Received: 24 January 2024
Revised: 13 February 2024
Accepted: 22 February 2024
Published: 26 February 2024

1. Introduction

Ship structural optimisation is integral to efficiently arranging components within a ship, reducing steel usage and ensuring structural integrity [1]. It is crucial for improving stress distribution, lowering maximum stress levels, and enhancing resistance in rough sea conditions while mitigating corrosion and structural failure risks. Concurrently, optimising the deadweight of a transport ship is vital for financial and operational viability, with lighter ships proving more advantageous, thus playing a pivotal role in increasing a ship's deadweight while reducing its lightweight for cost-effective construction [2]. Though ship design optimisation is complex, the focus is on lowering structural weight while preserving fundamental proportions. This method offers several benefits, including decreased fuel consumption, augmented deadweight capacity, improved freeboard, reduced initial costs, increased speed, and enhanced accessibility to channels and ports [3].

Objective function optimisation maximises and minimises problems under constraints. Structural optimisation, an essential design tool, has been a hot topic in engineering for decades. Formula-based structural design methods provide workable but not optimal designs. Therefore, the optimal structure or structural element approach must be chosen among the practical possibilities representing the genuine issue and yield reliable results [4]. Louvros, P. et al. (2022) employed a multi-objective optimisation strategy to design the internal layout of innovative ships. The potential of multi-objective optimisation in the first stages of innovative ship design is highlighted in the article. Additionally, it offers the user inherent control throughout the entire design process. The procedure seeks to find the best solutions for various design objectives by relocating ship components [5]. Pereira, T. and Garbatov, Y. (2022) developed a design procedure that integrates various factors to determine the optimal level of ship safety. This method encompasses innovative risk-based ship hull structural design, capital and operational expenditure, cargo capacity, and energy efficiency. The chosen design approach minimises costs and improves efficiency while increasing cargo capacity and reducing risks [6]. Pavlovic, A. (2020) explored a multi-step, multi-objective design methodology to optimise the photovoltaic roof of a multi-occupant racing vehicle. The study focused on selecting the most suitable composite structure while considering static strength and dynamic stiffness. [7]. Pavlovic, A. and Fragassa, C. (2020) investigated the optimisation of electro-mechanical devices for automatic gear changing using finite element method (FEM) simulations. Through analysing a commercial case study, the study emphasises the importance of combining theoretical models, computer simulations, and experimental approaches for accurate comprehension and decision-making in product development endeavours [8]. Raikunen, J. et al. (2019) presented a method to optimise the design of passenger ships during the early concept phase. A 3D finite element model was utilised to evaluate the response, with offset beam elements for the principal stiffeners and equivalent single-layer elements for the stiffened panels. The study found that relaxing the stress significantly impacted the ship's overall mass [9]. Andric, J. (2019) presented a ground-breaking methodology for decision support in ship structural design. Based on a multi-level Pareto optimisation strategy, the approach enables the simultaneous evaluation of numerous objectives and constraints. It combines three design phases to produce a variety of design options quickly, addressing topological (number of decks), structural (material and cross-section dimensions), and layout (compartmentation) aspects of the ship structure. The study illustrates significant improvements in structural performance and weight reduction when comparing the results to conventional design methods [10]. A.M.H. Elhewy et al. (2016) optimised an offshore supply vessel (OSV) using the blind search technique. Size structural optimisation reduced the vessel's steel weight and production cost by 42% without structural inadequacy. This weight reduction for a popular design, without altering dimensions, reduces fuel consumption and initial costs. It is a highly cost-effective choice because it improves access to the harbour, the canal, and the speed of the lightship [3]. Ma, M., O. Hughes, and J.K. Paik (2013) used the Pareto Simulated Annealing (PSA) algorithm for the tanker's multi-objective optimisation: minimising weight and cost while optimising buckling and stress. The model weight was reduced by 2.5% from 2,401,080 kg to 2,341,710 kg [11]. Motta, D. et al. (2011) used the LBR-5 programme for Multi Structures Optimisation of a Mega Yacht. The optimisation evaluation decreased cost (20%) and weight (8%) compared to the original scantlings. These data show that smaller ships benefit from structural optimisation [12]. Rigo, P., and the University of Liege (2003) developed an integrated LBR-5 programme to optimise vessel cost and weight. The optimisation tool analyses massive structures (100 panels, 900 design variables and 5000 constraints to cover up to 10 loading cases). The optimisation adds 3.4% to weight and saves 8.5% on hull tank construction costs [13]. Yu, Y.-Y. et al. (2010) developed an efficient ship structural optimisation technique. After the optimisation solution, the ideal panel thickness meets all strength requirements. However, the algorithm makes the structure slightly heavier. The improved structure meets shipbuilding technology requirements. Therefore, this optimisation strategy could enhance structural strength and

reduce material and labour costs [2]. J.-D. Caprace, F. Bair, and P. Rigo (2010) developed a method to improve new software and deliver the right scantling solution early in the design phase. They found that min-max may work better than weight optimisation for this vessel (i.e., manufacturing cost gain of 3% and a weight gain of 12%). They manually standardised this document's min-max solution after optimisation. Standardisation reduced the weight by 2.13% and production costs by 0.45% [14].

The study's focus on optimising ship hull structures, particularly open-deck configurations, addresses a significant gap in maritime research by recognising the unique challenges posed compared to closed-deck ships. By examining 12 critical structural elements that impact longitudinal strength, the study provides a comprehensive approach to enhancing ship performance while ensuring safety standards and cost-effectiveness compliance. The utilisation of advanced computational tools, notably the NSGA-II algorithm, significantly reduces weight and production costs, showcasing the innovative contribution of the study to the field. Moreover, the inclusion of open-deck ships in the analysis, along with applying the Fractional Factorial Design for parameter identification, underscores the novelty and practical applicability of the research. Additionally, a rigorous validation process ensures that the proposed designs meet industry standards, thereby highlighting the potential for real-world implementation and the profound impact on advancing the sustainability and competitiveness of the maritime industry.

2. Investigated Ship within the Study

This study focuses on a multipurpose cargo ship currently in operation. The ship has a single-screw diesel engine with a bulbous bow and transom. The ship's cargo hold is double-skinned, making it suitable for transporting various types of cargo, including bulk grain, containers, oversized freight, and regular cargo. BV, NR 467 Steel Ship Classification Rules ensure the analysed ship's structural strength. Table 1 provides a comprehensive overview of the key features of the multipurpose cargo ship.

Table 1. Principal particulars of the multipurpose cargo ship.

Items	Dimensions
Length overall	104.135 m
Length between perpendiculars	98.535 m
Breadth moulded	15.250 m
Depth	7.450 m
Design Draught	4.900 m
Scantling Draught	5.600 m
Propulsion	Self-propelled

This ship was constructed using a longitudinal frame configuration. Web frames are positioned at every second main frame interval. Figure 1 presents the midship section of the investigated ship.

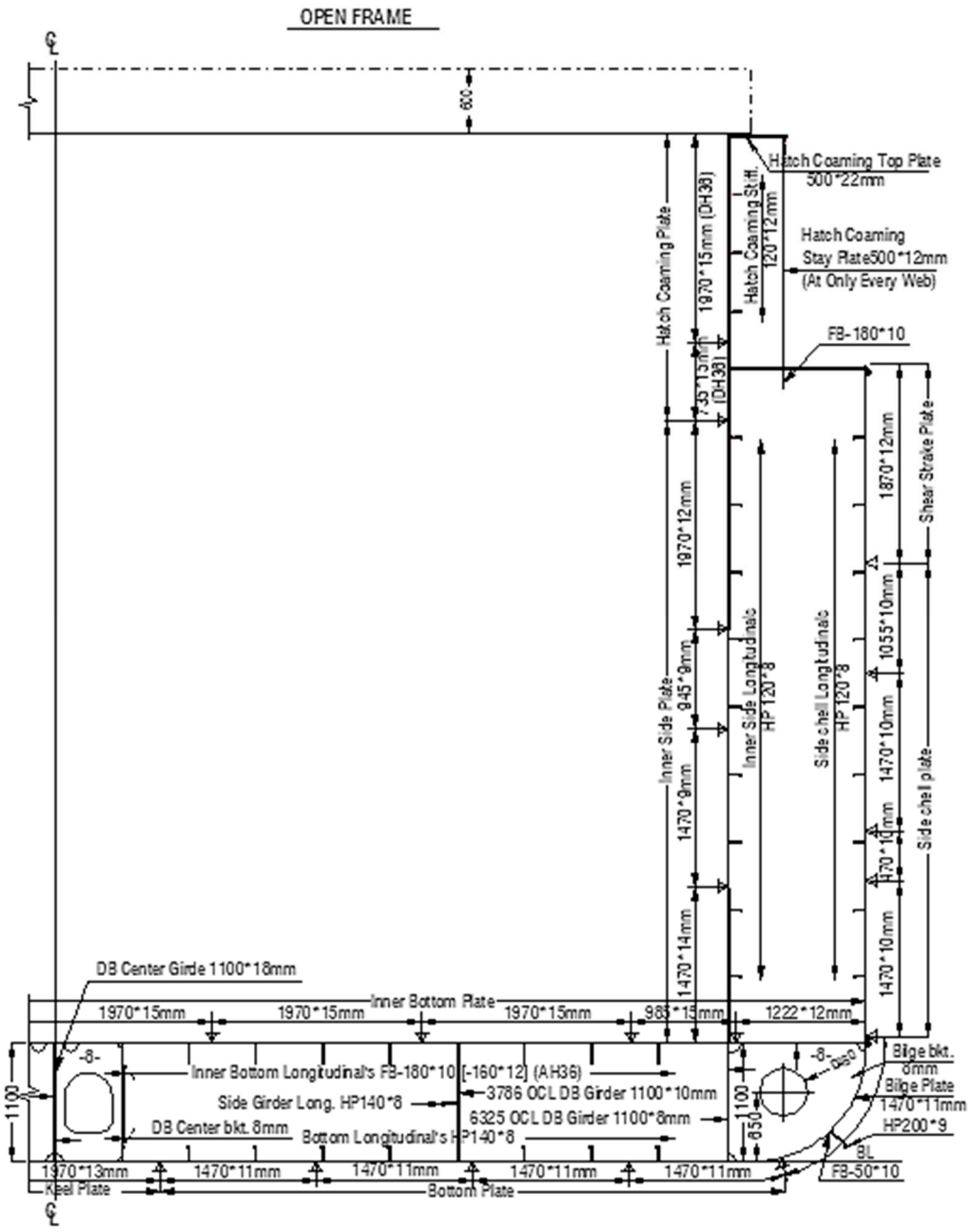

Figure 1. Midship section of the investigated ship.

2.1. Ship Hull Structural Analysis

The strength of the longitudinal hull girder members, primary supporting members, and transverse bulkheads is evaluated through cargo hold strength analysis.

2.1.1. Structural Model

There are four primary steps involved in creating a finite element model:

- geometry creation
- meshing and boundary conditions application
- solution
- examination of the findings

Figure 2 shows a detailed representation of the cargo hold model, including various connected parts such as frames and longitudinal stiffeners. This complex structure highlights the strength and effectiveness of the analysis system. Key measurements of the model

include an impressive analysed cargo hold length of 72.215 m, a forward hold length of 5.005 m, an aftward hold length of 9.6 m, a width of 15.25 m, and a height of 9.65 m. It is constructed with a relatively fine mesh consisting of 167,949 nodes and 211,530 elements, showcasing the precision and sophistication of the simulation.

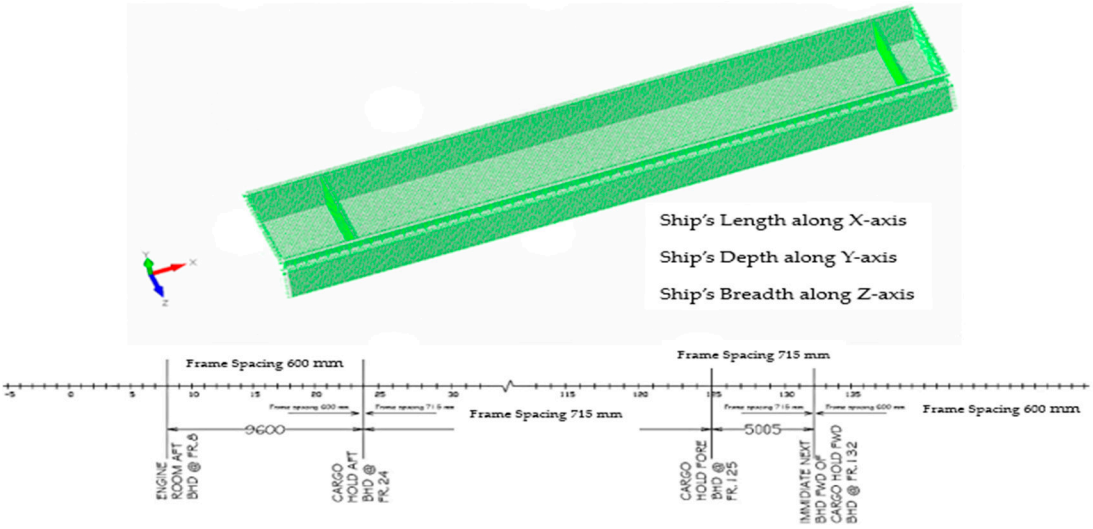

Figure 2. Generated FE model of the investigated ship in FEMAP.

The properties of the mesh system are as follows:

- One shell element between each stiffener;
- At least three elements across the depth of girders, floors, web frames, and stringers;
- Eccentric beams are used to represent all stiffeners.

2.1.2. Boundary Condition, Applications of Loads/Moments

If a cantilever beam has a bending moment on one side, the bending moment will be the same in all parts along the beam's length. The same concept was used in this FE-model to explore the longitudinal strength of the hull girder. On one side of the FE- model, bending moments were applied, while the other was restricted by fixed constraints (Table 2). Rigid elements were built beneath the main deck to transfer the load to the hull structure. A rigid element links the nodes at the free edges of the structure to the other nodes on the same plane, allowing them to function as a single entity. In order to establish two boundary conditions, it was necessary to utilise two rigid components:

1. Constraint: A rigid element was applied at the model aft with zero degrees of freedom to clamp.
2. Moment: To establish a hogging/sagging condition, a bending moment was applied in the positive y-direction to a rigid element in the fore part of the model [15].

Table 2. Boundary conditions.

Boundary Conditions	Translations in Directions			Rotation Around Axes		
	X	*Y*	*Z*	*X*	*Y*	*Z*
The node at the aft end	Fixed	Fixed	Fixed	Fixed	Fixed	Fixed
The node at the fore end	Free	Free	Free	Free	Free	Free

Figure 3 illustrates the behaviour of a cantilever beam subjected to a constant bending moment. Within a cantilever beam, the bending moment experiences maximum magnitude at the fixed end while progressively diminishing to zero at the free end.

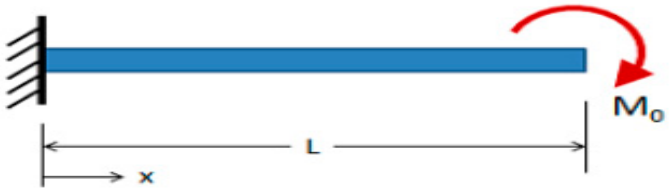

Figure 3. Cantilever beam applied with constant bending moment.

2.1.3. Checking Criteria for Stress

A strength check was performed with FEMAP, utilising checking criteria from BV and NR 467 rules to classify steel ships [16]. The master allowable stress, σ_{Master}, in N/mm^2, was obtained from the following formula:

$$\sigma_{Master} = \frac{R_y}{\gamma_R \gamma_M} \quad (1)$$

where:

R_y: is the yielding stress;

γ_R: is the resistance partial safety factor and

γ_M: is the material partial safety factor.

For mild steel (Grade A), the master allowable stress, σ_{Master}, is calculated as 219.42 N/mm^2. σ_{Master}, the maximum allowed stress for high tensile steel (Grade AH-36), is estimated to be 331.77 N/mm^2. It is necessary to confirm that the equivalent von Mises stress σ_{VM} is by the following formula for different types of analyses:

$$\sigma_{VM} \leq \sigma_{Master} \quad (2)$$

2.1.4. Analysed Ship Structural Analysis—Upright (Head Sea) Condition

In the analysis of ship structural integrity in the upright (head sea) condition, sagging has been identified as the worst-case scenario due to high hull girder stress in upright conditions (as seen in Figures 4 and 5) and a higher bending moment (refer to Table 3). Therefore, this study has chosen the sagging condition for further investigation. When a ship is upright, it will experience both still water and vertical wave bending. Analysing stress values in the midship regions is crucial to evaluating the ship's structural strength and integrity. The midship section is a critical structural parameter determining the ship's ability to withstand bending stresses.

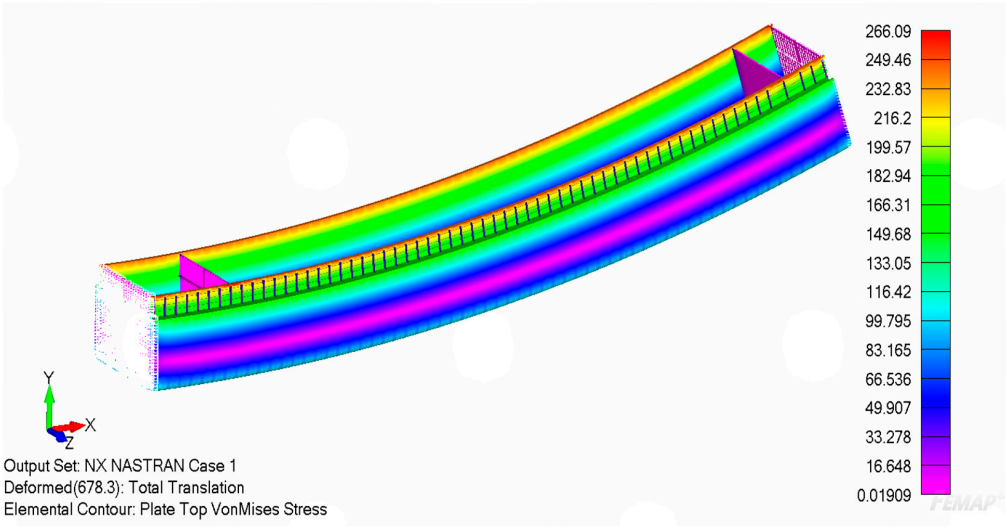

Figure 4. Hull girder von Mises stress (MPa) at midship (sagging—upright condition).

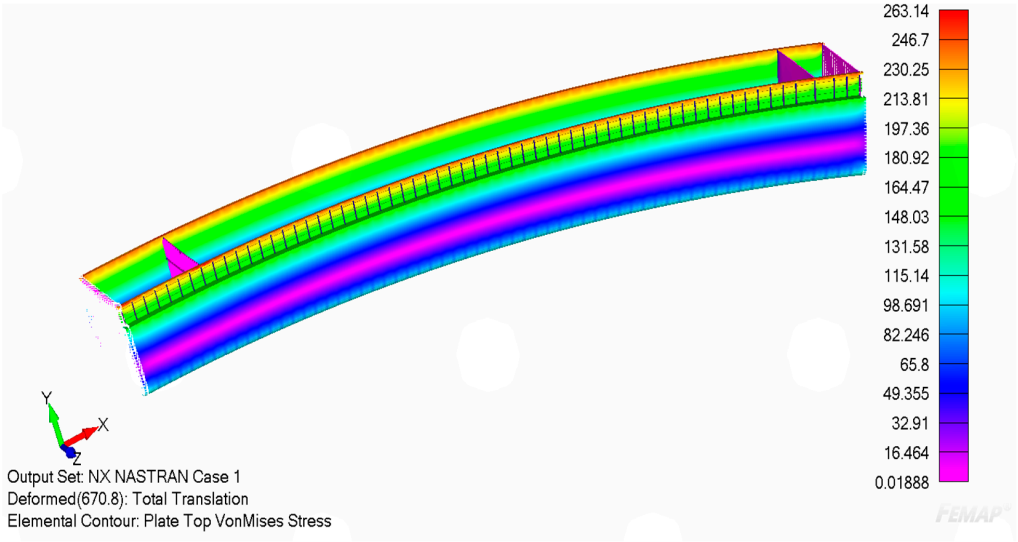

Figure 5. Hull girder von Mises stress (MPa) at midship (Hogging—upright condition).

Table 3. Hull girder strength criteria.

Items	Hogging (kNm)	Sagging (kNm)
Design still water bending moment	125,651	−113,909
Design vertical wave bending moment	177,581	−192,769

Figures 4 and 5 provide a detailed analysis of the structural integrity in both sagging and hogging scenarios under upright conditions. The study indicates that the peak stress level recorded in the sagging scenario is 266.09 MPa, while in the hogging scenario, it is slightly lower at 263.14 MPa. It is essential to note that the highest stress levels remain significantly below the maximum allowable limit in both critical load cases. This observation ensures that the analysed system is structurally robust and can tolerate the applied loads while ensuring safety and reliability within acceptable parameters.

2.1.5. Mesh Sensitivity Analysis

Mesh sensitivity analysis is a numerical simulation technique to obtain precise results by determining the best mesh size and quality. It involves varying the mesh size and comparing the simulation results to find the optimal mesh size for the desired accuracy. This technique is employed in ship modelling to study the impact of mesh size and quality on the accuracy of the simulation results. By conducting mesh sensitivity analysis, the precision of the simulation can be enhanced, and the behaviour of the ship model can be better understood under different conditions.

The convergence curve shown in Figure 6 demonstrates that the Mesh Density factor of 0.0028 makes the results stable, confirming the chosen model's accuracy. This factor is crucial in determining the most suitable mesh size for a given simulation.

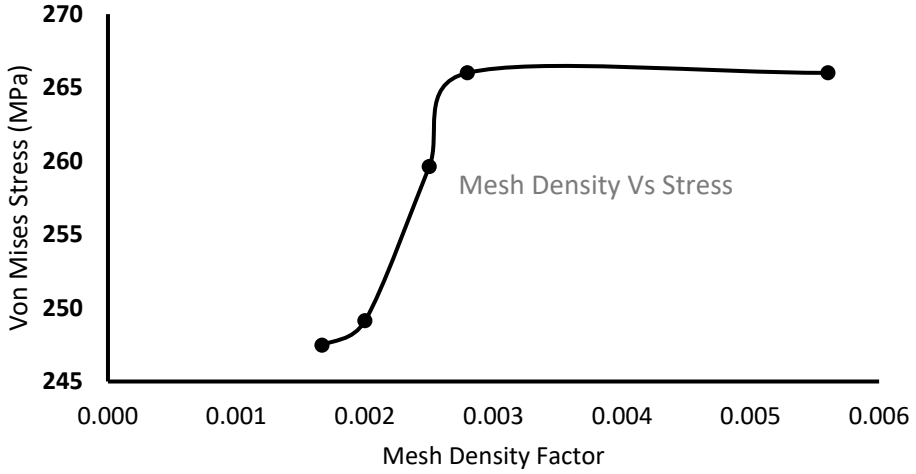

Figure 6. Convergence curve illustrating optimal mesh density for simulation accuracy.

3. Design of Experiment (DOE)

Design of Experiments (DOE) is a structured method applied across various domains, such as engineering, manufacturing, and scientific research, to conduct experiments systematically. It entails carefully planning experimental setups to ensure reliable and valid results while optimising resource utilisation. By controlling sources of variation, DOE enables researchers to understand the relationship between input factors and output responses. Statistical methods utilised in DOE aid in process optimisation, quality improvement, and cost reduction. Additionally, DOE is crucial for identifying significant factors and their interactions, contributing to developing robust and efficient systems. Overall, DOE is a valuable tool for advancing knowledge and innovation across diverse fields by providing a structured framework for experimentation and analysis [17].

DOE aims to optimise the model by selecting the optimal elements and levels. Project teams can apply different values to important model factors to gain more model information. The DOE results provide maximum information with minimal resources. Depending on how factor levels affect DOE outcomes, variables can be categorised to identify which affect the average, both average and variability or have no effect on the quality attributes of DOE. DOE experiments may yield [18]:

1. Identification of critical variables affecting the outcome (s) of the DOE.
2. Establishment of factor(s) levels for important components optimising the intended result.
3. Selection of the optimal or most cost-effective configurations for insignificant elements.
4. Validation (confirmation) of responses and incorporation into production or design.

3.1. Plackett–Burman Design

The Plackett–Burman design (PBD) is a valuable screening technique to identify significant elements from many variables influencing a given process. This research focused on twelve variables, including primary and secondary structural members and overall structural strength. Applying the PBD was instrumental in pinpointing the pivotal variables requiring a thorough investigation [19].

The two-level factorial design, pioneered by Plackett and Burman, has found application in analysing diverse medium elements and environmental conditions. At its core, the first-order model forms the foundation of the Plackett–Burman framework:

$$Y = \beta_0 + \Sigma\beta_i X_i \quad (3)$$

where Y is the predicted response, β_0 is the model intercept, β_i is the linear coefficient, and X_i is the level of an independent variable. In the scope of this present research endeavour, a comprehensive investigation encompassing twenty distinct experimental designs, each

featuring twelve assigned variables, was conducted. The assessment of the significance of these factors hinged on the criterion that their confidence intervals attain a threshold of 90% or higher [20].

Figure 7 illustrates Plackett and Burman's screening approach to investigate 12 factors through 20 experimental runs. These factors are evaluated at two levels: higher (+) and lower (−). The main goal of this method is to identify and measure the effects of each factor on the target parameter. The Plackett/Burman plan provides researchers with a reliable framework for conducting thorough foundational analyses.

Run	Block	A	B	C	D	E	F	G	H	J	K	L	M
1	1	–	–	+	+	−	+	+	−	−	−	−	+
2	1	+	+	−	−	+	+	−	+	+	−	−	−
3	1	+	−	−	+	+	−	+	+	−	−	−	−
4	1	−	+	+	+	+	−	−	+	+	−	+	+
5	1	+	−	−	−	−	+	−	+	−	+	+	+
6	1	+	−	+	+	−	−	−	−	+	−	+	−
7	1	−	+	−	+	−	+	+	+	+	−	−	+
8	1	+	+	−	−	−	−	+	−	+	−	+	+
9	1	+	+	−	+	+	−	−	−	−	+	−	+
10	1	−	−	−	−	+	−	+	−	+	+	+	+
11	1	+	+	+	−	−	+	+	−	+	+	−	−
12	1	−	+	+	−	−	−	−	+	−	+	−	+
13	1	−	−	−	−	−	−	−	−	−	−	−	−
14	1	−	−	−	+	−	+	−	+	+	+	+	−
15	1	−	+	+	−	+	+	−	−	−	−	+	−
16	1	+	+	+	+	−	−	+	+	−	+	+	−
17	1	+	−	+	−	+	+	+	+	−	−	+	+
18	1	−	−	+	−	+	−	+	+	+	+	−	−
19	1	+	−	+	+	+	+	−	−	+	+	−	+
20	1	−	+	−	+	+	+	+	−	−	+	+	−

Figure 7. Plackett and Burman's Screening Scheme for Investigating 12 Factors.

3.2. Fractional Factorial Design

Fractional factorial studies decrease the size of an experiment by not analysing all variable levels.

The number of experiments N necessary for a thorough factorial design examination is supplied as follows:

$$N = L^F \tag{4}$$

The number of levels is L, while the number of factors is F. Thus, the FEM model performed many calculations. Fractional factorial designs reduce measurements, and these models only consider some possible element combinations, and Plackett and Burman's screening strategies analyse just a fraction of them [21].

4. Analysis of Key Ship Variables and Their Effects on Hull Integrity and Production Costs

The following factors are considered for the examination of the analysed ship's hull integrity:

Thickness of

- Keel plate
- Bottom plate
- Side shell plate
- Shear strake plate
- Inner bottom plate
- Inner side shell plate
- Main deck plate
- Hatch coaming plate
- Hatch coaming top plate
- Double bottom longitudinal girder, CL

Spacing of

- Web Frame
- Stiffener

A detailed study was conducted to investigate the effect of hull girder von Mises stress on the integrity of ship hulls. The complex analysis results are concisely presented in Figure 8, visually depicting the significant impact of von Mises stress on the hull.

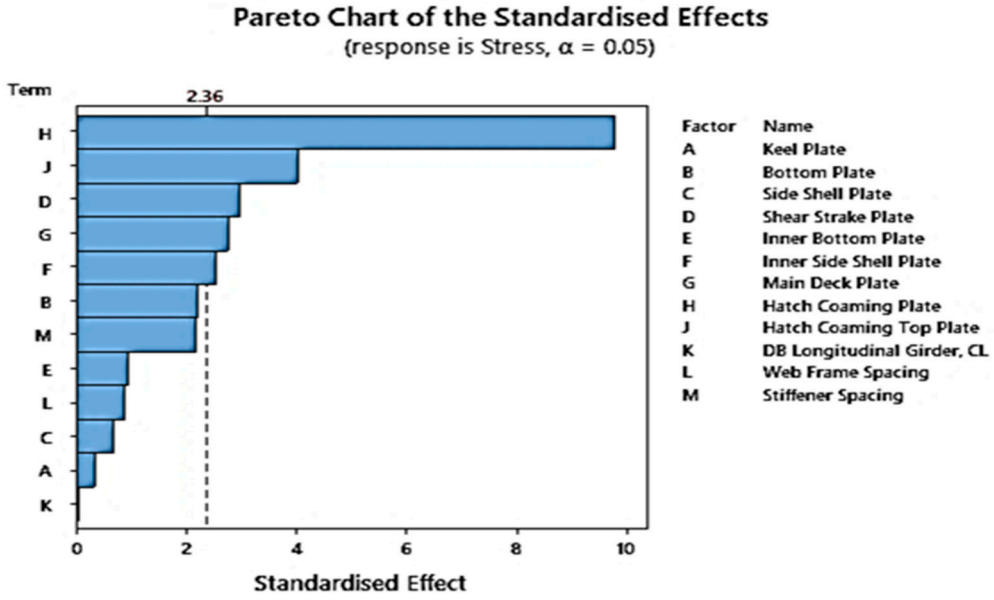

Figure 8. Utilising the Plackett–Burman screening plan to determine the primary effects of von Mises stress (MPa) on ship hull girders.

The Pareto diagram prominently identifies the top five critical factors that affect the hull integrity, namely:

- Hatch coaming plate
- Hatch coaming top plate
- Shear strake plate
- Main deck plate
- Inner side shell plate

The factors mentioned above are further evaluated in depth using a fractional factorial design on two levels, allowing interaction between the components.

The primary and interaction effects depicted in Figure 9 strongly agree with the main effects identified in the screening plan presented in Figure 8. This observation suggests that screening plans are valuable tools for initial assessments. Furthermore, Figure 8 highlights additional significant factors and emphasises the importance of their interactions. The diagram reveals that the following five factors are of utmost significance:

- Hatch coaming plate
- Hatch coaming top plate
- Main deck plate
- Shear strake plate
- Bottom plate

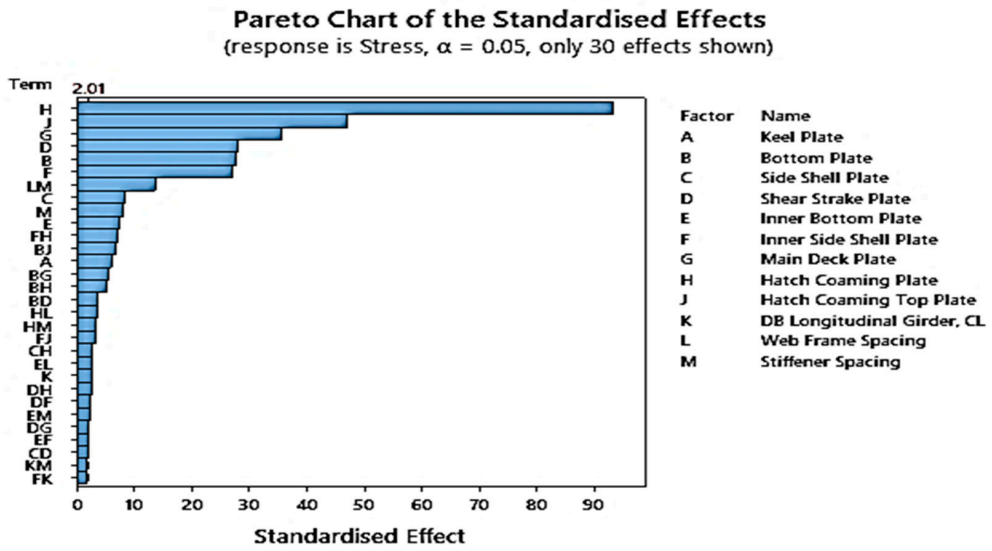

Figure 9. Visualisation of standardisation effects on stress response: Pareto chart analysis.

Table 4 presents a detailed overview of the regression model's key performance metrics in this research. These metrics offer critical insights into the model's efficacy.

$$\begin{aligned}\text{Regression Equation (von Mises Stress)} = {} & 935.3 - 2.58A - 11.21B - 3.21C - \\ & 5.60D - 4.69E - 2.10F - 4.37G - 6.09H - 5.68J - 1.78K - 0.1504L - 0.3567M + 0.0007AB \\ & - 0.0281AC + 0.0235AD - 0.0042AE - 0.0355AF - 0.0170AG + 0.0281AH + 0.0256AJ \\ & - 0.0218AK + 0.000266AL + 0.00270AM - 0.0366BC + 0.1120BD + 0.0406BE - 0.0224BF + \\ & 0.1475BG + 0.1402BH + 0.1798BJ - 0.0097BK + 0.00059BL + 0.00086BM + 0.0608CD - \\ & 0.0433CE - 0.0106CF - 0.0004CG + 0.0719CH + 0.0440CJ - 0.0364CK + 0.000228CL + \\ & 0.00236CM + 0.0151DE + 0.0602DF + 0.0540DG + 0.0682DH + 0.0086DJ + 0.0240DK - \\ & 0.000152DL - 0.00191DM - 0.0464EF - 0.0267EG + 0.0322EH + 0.0169EJ + 0.0013EK + \\ & 0.000531EL + 0.00470EM + 0.0100FG + 0.1580FH + 0.0736FJ - 0.0323FK - 0.000284FL - \\ & 0.00255FM - 0.0184GK + 000087GL + 0.00076GM + 0.0160HK - 0.000652HL - \\ & 0.00651HM - 0.0009JK + 0.000013JL - 0.00150JM + 0.000268KL + \\ & 0.00291KM + 0.000219LM\end{aligned} \quad (5)$$

Table 4. Model summary (hull girder stress).

S	R-Squared	R-Squared (adj)	R-Squared (pred)
2.24154	99.66%	99.17%	97.94%

Figure 10 provides crucial insights into the normalcy assumption through the standard probability plot of residuals. The plot illustrates the validity of the normality assumption, as the residuals exhibit a close adherence to a linear pattern.

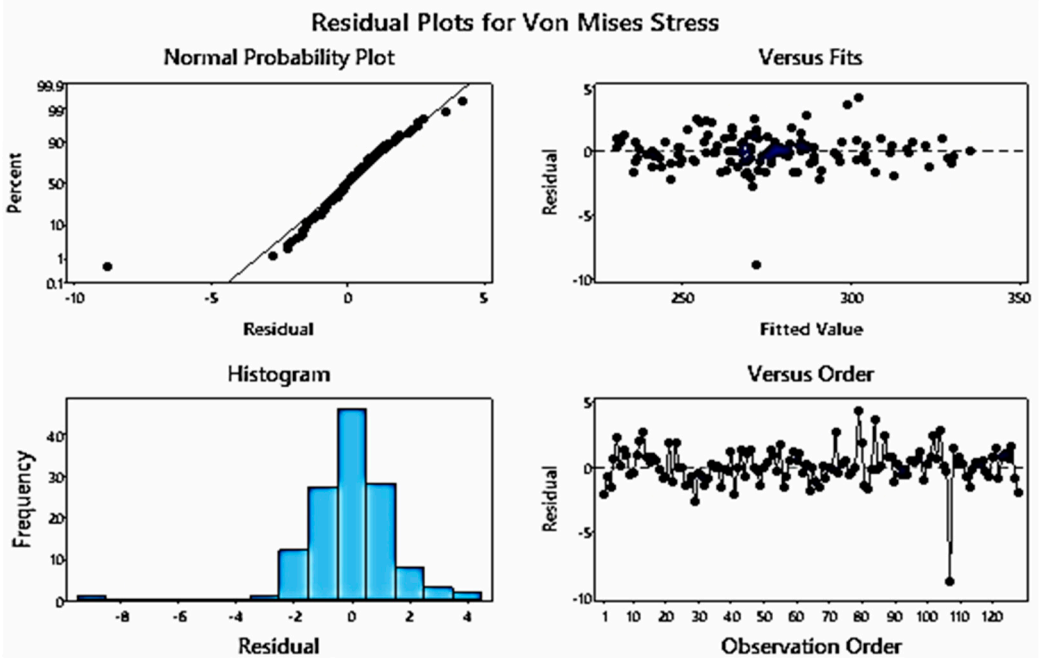

Figure 10. A residual plot for hull girder stress analysis and visualisation.

In ship structure design, it is essential to consider the impact on production costs, as shown in Figure 11. The analysis conducted identified the top five factors that significantly affect production costs:

- Inner bottom plate
- Inner side shell plate
- Bottom plate
- Web frame spacing
- Side shell plate

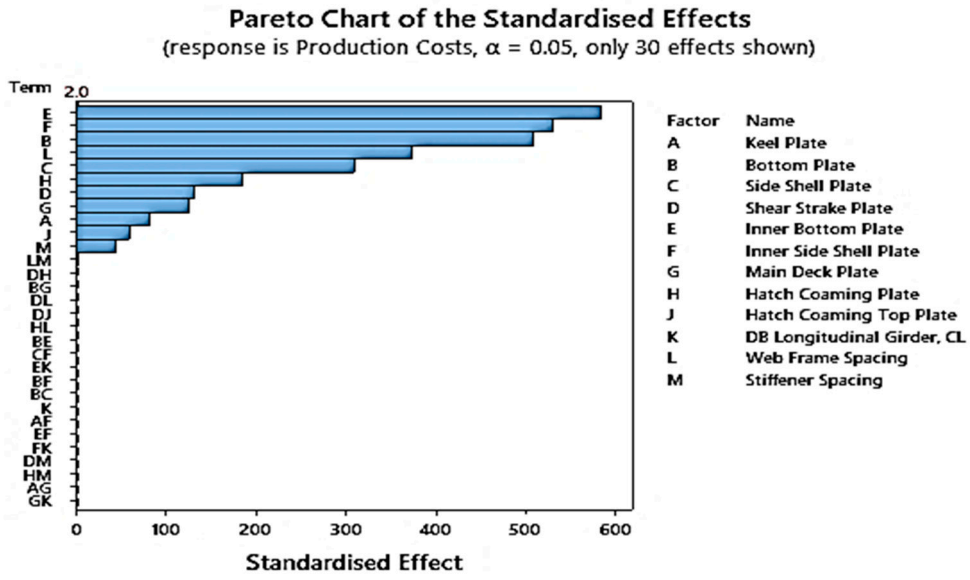

Figure 11. Visualisation of standardisation effects on production costs response: Pareto chart analysis.

As previously mentioned, a comprehensive examination of the interactions between these components was also conducted. In this specific context, it is noteworthy that no significant interactions among the elements were observed.

Table 5 displays important metrics for evaluating the effectiveness of the regression model used to analyse the production costs of ships in this study, providing valuable insights into the model's performance.

Table 5. Model summary (production costs).

S	R-Squared	R-Squared (adj)	R-Squared (pred)
1518.24	100.00%	99.99%	99.97%

Figure 12 displays the residual plots, which are crucial for evaluating the model's goodness of fit and detecting any discernible patterns or trends within the residuals. These plots are essential in validating whether the statistical models' assumptions hold true.

Regression Equation (Production Costs) = 892606 + 4557A + 25778B + 15108C + 8445D + 29447E + 22487F + 6468G + 7193H + 3720J − 1100K − 122.71L − 111.1M + 19.1AB + 19.1AC − 16.4AD − 17.5AE + 16.1AF − 16.1AG + 13.7AH − 13.5AJ + 13.8 AK − 0.115AL − 1.18AM − 23.3BC + 19.9BD + 21.2E − 19.4BF + 19.5BG − 16.2BH + 16.5BJ − 16.4BK + 0.134BL + 1.38BM + 19.7CD + 21.0CE − 19.4CF + 19.2CG − 16.3CH + 16.5CJ − 16.5CK + 0.138CL + 1.41CM − 18.0DE + 16.5DF − 16.3DG + 20.2DH − 19.5DJ + 14.0DK − 0.163DL − 1.68DM + 17.6EF − 17.4EG + 14.8EH − 15.1EJ + 15.1EK − 0.125EL − 1.29EM + 16.0FG − 13.6FH + 13.6FJ − 13.8FK + 0.114FL + 1.18FM + 13.8GK − 0.116GL − 1.19GM − 11.7HK + 0.136HL + 1.40HM + 11.8JK − 0.134JL − 1.38JM + 0.099KL + 1.01KM − 0.0240LM (6)

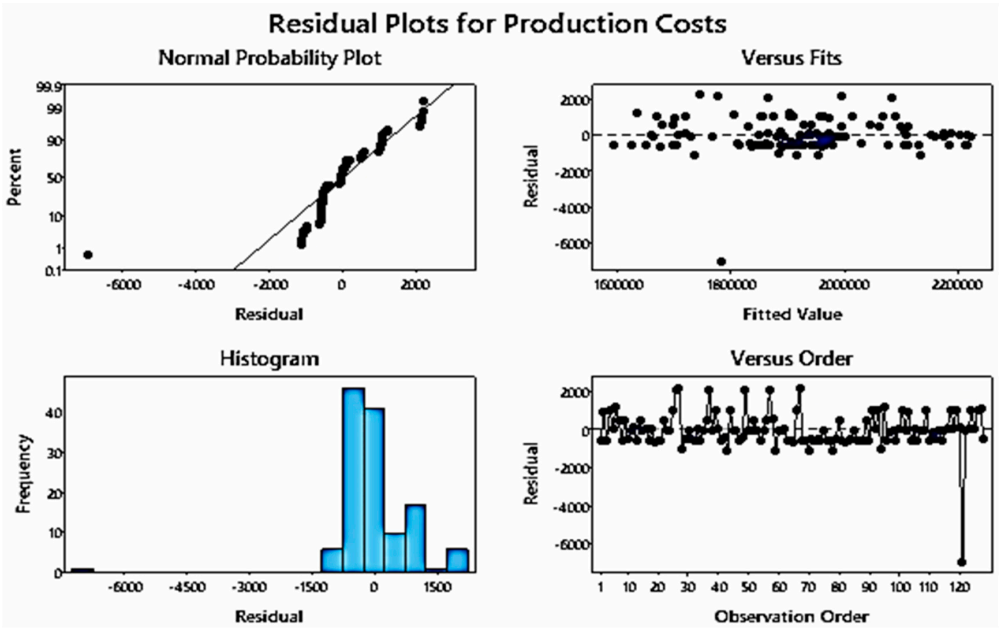

Figure 12. A residual plot for production costs analysis and visualisation.

5. Structural Optimisation Tools

Objectives functions, design variables, constraints, and an optimisation algorithm are needed to optimise ship structures like many other optimisation tools.

5.1. Objective Functions

Objective functions are assessed using numerical or mathematical expressions and rely on design variables. Objective functions include weight, manufacturing cost, life-cycle cost, and safety index. The two objectives of this application are production costs and minimum weight.

5.1.1. Hull Structure's Weight

A challenging problem involving the link between the number of structural elements in the longitudinal and transverse directions and their dimensions, which affect the structural weight, must be solved to optimise the ship's structural topology. Constraints relating to the ship's construction and functioning requirements should also be considered. The objective function $f(x)$ for optimising the weight of the hull structure is expressed as follows:

$$f\ (x) = \sum_{j}^{r} w_j\ SW_j;\ r = 9 \tag{7}$$

where:

r—number of structural regions
SW_j—the j-th structural region's structural weight
w_j—the relative weight coefficient (also known as the relative importance of structural weight) of the various regions varies [22].

5.1.2. Production Costs

The production costs (PC) are subdivided into three categories:

- the raw materials costs (MC)—Quantifying the volume needed for construction and receiving pricing from suppliers and subcontractors are the first steps in evaluating material costs.
- the labour costs (LC)—Analytical evaluation is the best option for empirical formulations for evaluating labour costs. Such a strategy necessitates understanding the amount of time needed to complete each typical labour task connected to a workstation and the split of the entire construction process into stations.
- the overhead costs (OC)—overhead costs are all costs related to construction that cannot be directly connected to a particular workstation in the construction process.

$$PC = MC + (LC \times HC) + OC \tag{8}$$

where, PC is the production cost (€); MC, material cost (€); LC, labour cost (man-hours); HC, hourly cost (€/hour); OC, overhead costs (€) [14].

5.2. Design Variables

The principal structural dimensions can serve as design variables and localised characteristics, such as the stiffener web thickness within a given structural area, whether applied to the entire structure or just a particular segment. "Design variables" refer to various characteristics, including material type, grade, stiffener configurations (bulb, T, and L), overall deck section, and other relevant elements.

The scantling of these stiffened panels is an important design factor. Despite widespread efforts to standardise production efficiency, there are differences amongst panels in the scantlings. The particular panel scantling, for example, HP-200 or FB-100×10, impacts plate thickness, frame spacing, stiffener spacing, and stiffener dimensions [22].

5.3. Design Constraints

Constraints can be categorised as either explicit or implicit functions of design variables, which may take on linear or non-linear forms. These constraints are mathematical expressions that encapsulate user-imposed limitations on design variables, encompassing aspects such as displacement, stress, ultimate strength, and more [14].

5.4. Optimal Solution

An optimal solution minimises or maximises the objective function and is possible. The decision maker can choose Pareto front design solutions for multi-criteria optimisation problems based on trade-offs [23].

6. Multi-Objective Optimisation

The multi-criterion optimisation problem involves $K > 1$ criteria and can be formulated as

$$min_x F(X) = [F_1(X),\ F_2(X), \ldots F_K(X)] \tag{9}$$

$$X = [X_1,\ X_2,\ \ldots X_N\ ]^T$$

subject to constraints on both equality and inequality

$$h_i(X) = 0,\ \ i = 1, \ldots, \mathrm{I}$$

$$g_i(X)\ \geq\ 0,\ \ j = 1, \ldots, \mathrm{J}$$

with K multiple optimisation criteria, $F_1(X)$ through $F_K(X)$ now exist, and each depends on the N unknown design variables in the x-vector. Now, a vector F represents the total objective function. Due to K criteria conflicts, this problem has no single solution [24].

6.1. Pareto Optimum Front

A Pareto optimal solution is one where no individual can be improved without worsening the position of at least one other participant [25]. The set of Pareto optimal solutions in multi-objective optimisation is called the Pareto optimal front, also known as the Pareto front or Pareto frontier. It illustrates the trade-offs when pursuing different goals, where achieving one objective may require sacrificing another. This makes it an essential resource for decision-making [26].

NSGA-II is an evolutionary algorithm that uses an elitist approach to identify Pareto optimal solutions by eliminating dominated alternatives. The Pareto front, representing trade-offs among multiple objectives, is constructed through this process [27]. Graphically, the Pareto front can be depicted as a curve or surface in the objective space, with each point on the curve signifying a Pareto optimal solution. To maintain population diversity, NSGA-II employs a crowding distance metric and a non-dominated sorting procedure to rank solutions based on non-dominance. The algorithm extracts the Pareto optimal front from the final population of solutions, which can be portrayed as a curve or surface in the objective space [28].

Figures 13 and 14 depict the "Feasible Solution Space", encompassing all viable solutions meeting specified constraints and objectives, and the "Pareto Optimal Curve", which identifies the optimal compromise solutions where no objective can be improved without sacrificing another. These visuals are vital tools in multi-objective optimisation, enabling decision-makers to navigate scenarios involving multiple, potentially conflicting objectives effectively and make informed choices that strike an optimal balance among them.

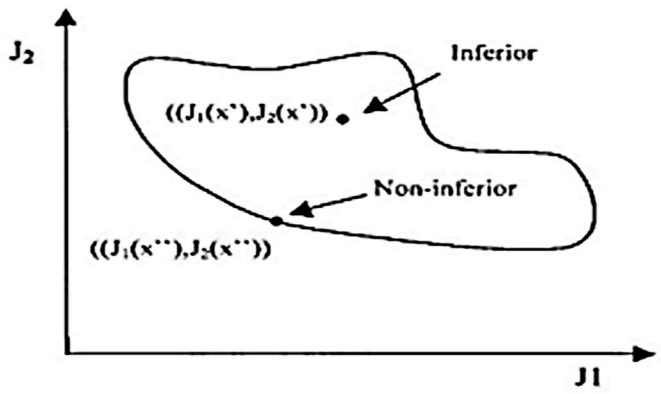

Figure 13. Feasible solution space [25].

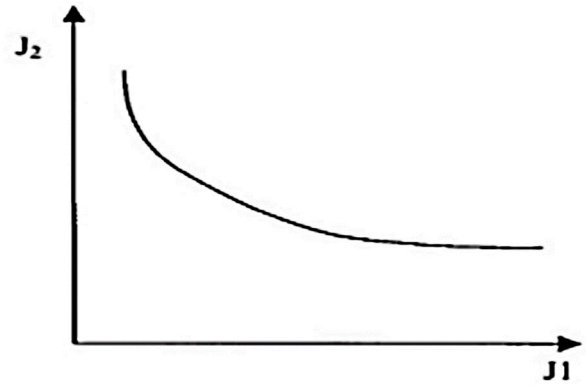

Figure 14. Pareto optimal curve [25].

6.2. Utilising NSGA-II Algorithm for Multi Objective Optimisation

For the Stop-Sweep approach, NSGA-II was chosen to obtain Pareto optimal solutions. This algorithm provides various configurable parameters, including population size (pop_size) and the number of generations (n_gen), which can be adjusted to control solution set density [29]. This study used a population size of 128 and a generation size of 500.

Design Optimisation for the Analysed Ship

This study aims to optimise a multi-purpose cargo ship based on two primary objective functions: minimising structural weight and reducing production costs. Employing a fractional factorial design approach and the NSGA-II algorithm implemented in Python, twelve independent design variables are utilised, each identified as a significant influencing factor.

The NSGA-II algorithm is employed in Python to optimise multiple objectives in designing a cost-effective and safe multipurpose cargo ship. Specifically, the algorithm is applied to determine the optimal thicknesses and spacing of web frames and stiffeners through a rigorous series of iterative processes while minimising production costs and the ship's weight, all within predefined constraints. Ultimately, this research will contribute to enhancing ship design and efficiency.

Two regression equations related to von Mises stress and production costs are integrated into the NSGA-II algorithm, derived carefully from analysing 128 model sets using Minitab. Random output values are thoughtfully incorporated to enhance the quality of the results.

7. Case Study 1

The structure is represented by stiffened panels (plates and curved shells). Each panel may be connected with up to nine (9) design variables. The following design parameters are listed:

- Plate thickness.
- For longitudinal members (stiffeners, crossbars, longitudinal, girders, etc.):
  - web height and thickness,
  - flange width,
  - spacing between two longitudinal members.
- For transverse members (frames, transverse stiffeners, etc.):
  - web height and thickness,
  - flange width,
  - spacing between two transverse members.

Figure 15 provides a detailed cross-sectional view of the midship, highlighting 27 stiffened panels within the section. This visual representation is vital for structural optimisation, offering crucial insights into hull design and construction.

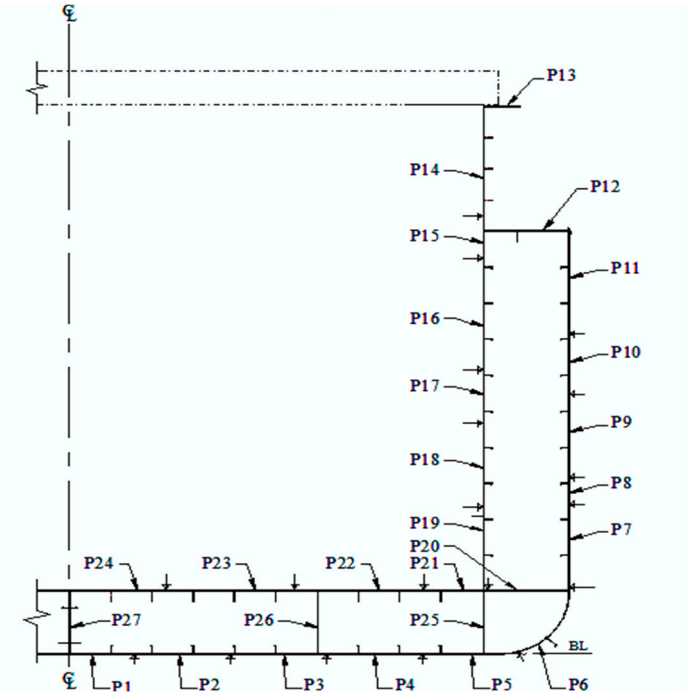

Figure 15. Panel definition of midship section.

The mesh model of the multipurpose cargo ship unit consists of the following elements:

- 27 stiffened panels in total, each with nine (9) different design variables
- Two additional panels to represent the symmetry axis (or boundary conditions)
- 243 design variables (9 × 27 panels)
- 54 equality constraints between design variables
- 243 geometrical constraints (9 × 27 panels)
- 486 structural constraints (243 by load case)
- Two constraints on hull ultimate strength

8. Case Study 2

This study conducted a comprehensive analysis to evaluate the costs associated with the production processes for manufacturing steel hulls. The production costs of the analysed ship were estimated using empirical formulas [30] within Microsoft Excel. Factors such as steel plate cost, work preparation cost, cutting cost, transport cost, forming cost, assembly cost, and welding cost were considered. Data on these costs were gathered from multiple Bangladeshi shipyards, including Ananda Shipyard and Slipways Limited, Three Angle Marine Limited, Western Marine Shipyard Limited, Radiant Shipyard Limited, and Karnafully Shipyard Limited. Ananda Shipyard and Slipways Limited was the reference point for comparison due to its involvement in the analysed ship's construction.

The analysis depicted in Figure 16 provides a detailed breakdown of the costs associated with fabricating steel hulls. The data indicate that a significant portion, precisely 39%, of production costs is allocated to procuring steel plates. Welding and cutting costs account for 19% and 10% of the overall costs, respectively, while forming, assembly, and work preparation costs each contribute 9% to the production process. Despite comprising only 5% of the total production costs, transport expenses still warrant attention due to their notable contribution.

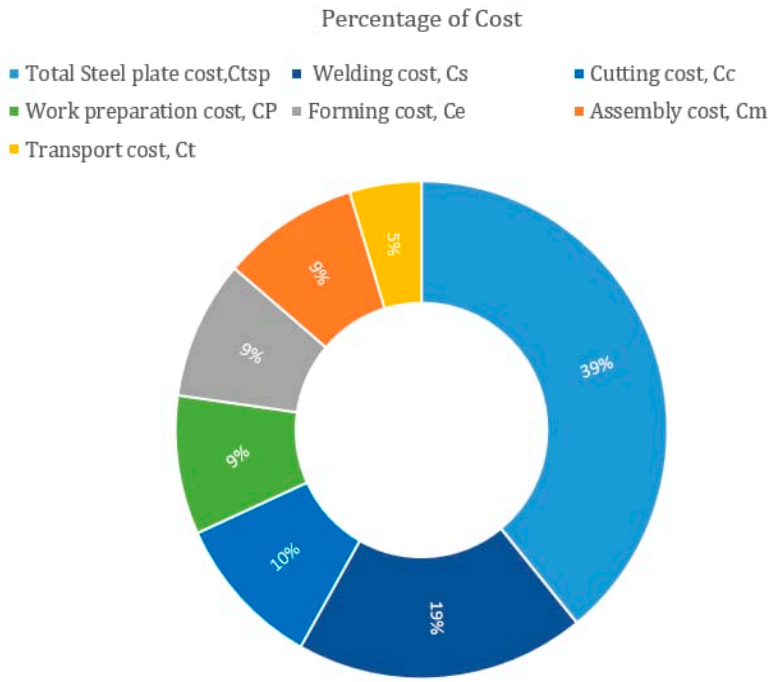

Figure 16. Distribution of production costs for the analysed ship.

9. Results and Pareto Front

Figure 17 is a multi-history chart showing the relationship between the number of iterations and the ideal hull girder von Mises stress parameter values in ship optimisation. This visual representation offers a valuable resource for researchers, engineers, and designers optimising ship scantlings. The analysis shows two significant optimisation milestones, one around the 190th iteration and another around the 490th iteration. At these points, the carefully adjusted dimensions of the ship's structure achieve a remarkable balance. Within this balance zone, the hull girder von Mises stress values remain consistently between 295 MPa and 299.8 MPa, which is quite impressive. This achievement reflects the precision and effectiveness of the optimisation process.

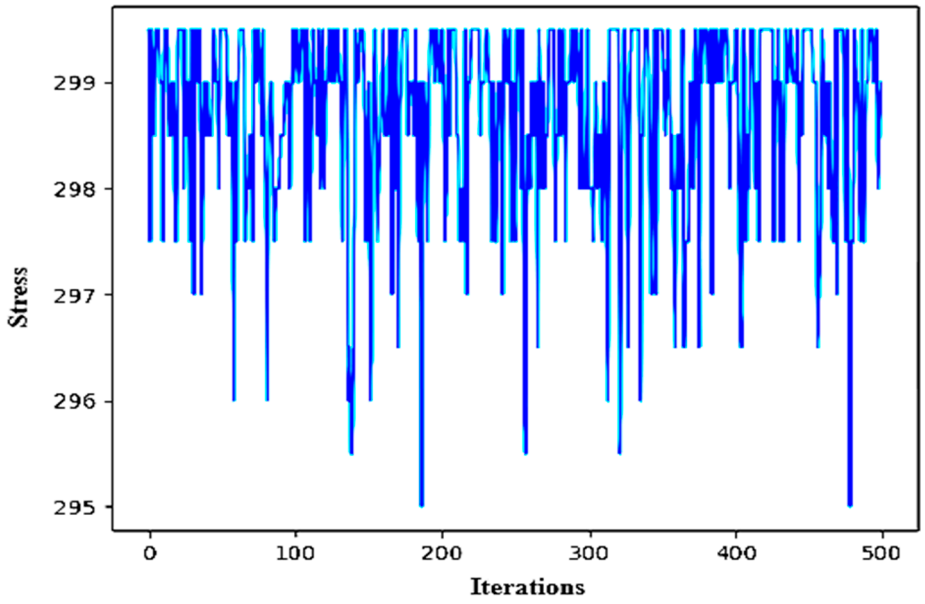

Figure 17. Number of iterations vs. best individual stress value.

Figure 18 offers a comprehensive visual representation of the iterative optimisation process and its impact on the ideal production costs of the analysed ship, providing valuable insights into the convergence and variation patterns. The chart showcases a multi-history perspective, tracking the relationship between the number of iterations and the corresponding ideal production cost values. Notably, the research reveals specific milestones within the iterative process where distinct trends emerge. Around the 140th and 480th iterations, the production cost estimates for the optimised ship reach a convergence point, stabilising at an upper threshold of approximately €2,035,000.

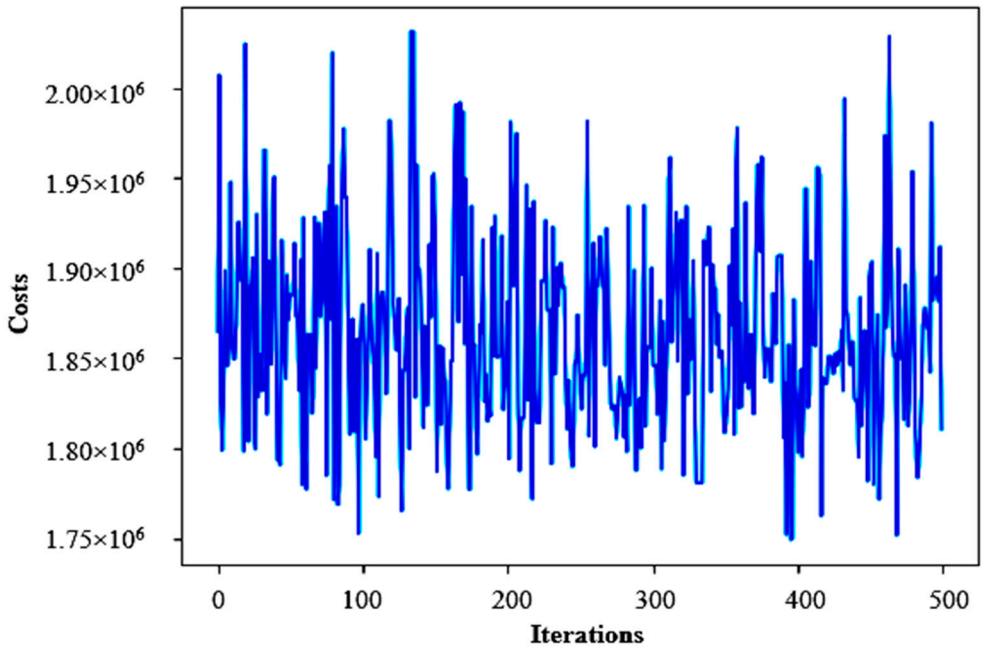

Figure 18. Number of iterations vs. best individual production cost value.

Conversely, the Figure demonstrates a noticeable decline at approximately the 100th, 400th, and 480th iterations, reaching a minimum threshold of approximately €1,750,000. These inflexion points represent critical junctures in the optimisation process, indicating substantial improvements in cost-effectiveness and highlighting the efficacy of the applied methodology.

Figure 19 displays the Pareto optimal curve, illustrating the relationship between production cost values and hull girder stress values for the optimised analysed ship. This graph is a crucial tool for designers and decision-makers, providing an intuitive way to navigate the complex trade-offs between structural integrity and cost-effectiveness. In this context, the Pareto optimal curve outlines the Pareto front, a set of non-dominated solutions in the multi-objective optimisation landscape. In this research, the Pareto optimal frontier occurs at a hull girder stress value of 296.2 MPa, corresponding to a production cost of about €1,770,000. The convergence point highlighted in Figure 19 provides an excellent solution that balances strong structure and cost-effectiveness.

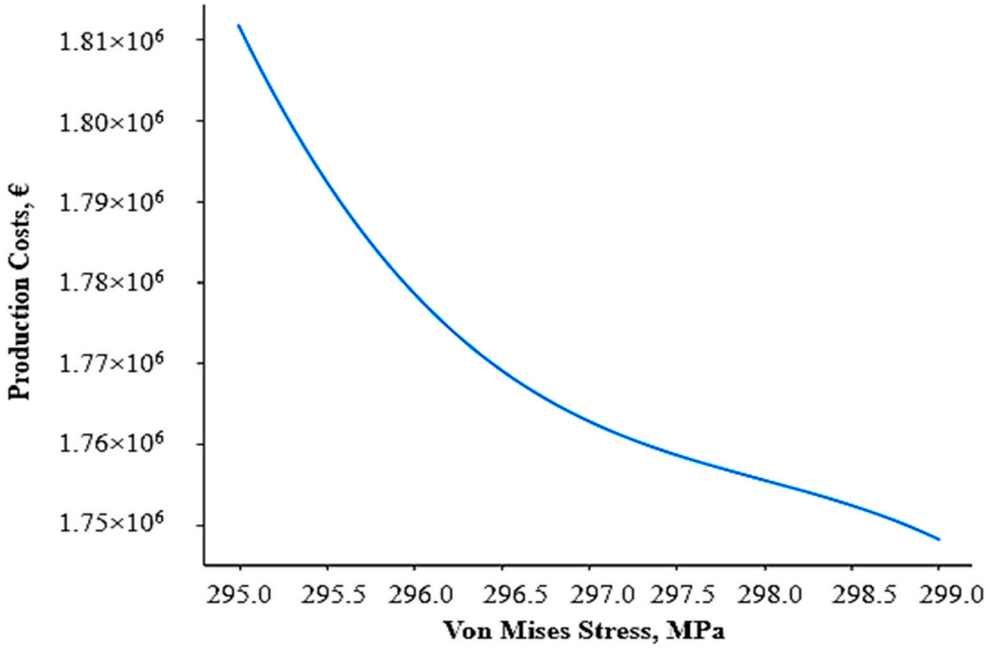

Figure 19. Pareto optimal curve: production costs vs. stress.

Table 6 provides a concise comparison of critical factors in cargo hold design. It lists components and their corresponding original and optimised net thickness, the initial and optimised cargo hold weight, and production costs. The "Original Net Thickness" and "Optimised Net Thickness" columns reflect changes in material thickness made during the optimisation process. Conversely, the "Original Cargo Hold Weight" and "Optimised Cargo Hold Weight" columns illustrate weight variations before and after design enhancements. Lastly, the "Original Production Costs" and "Optimised Production Costs" columns offer insights into cost reductions achieved through optimisation. This table serves as a valuable reference for decision-makers, enabling them to evaluate the overall impact of design changes on cargo hold parameters and production costs.

Table 6. Comparison of original and optimised parameters for cargo hold design.

Items	Original Net Thickness (mm)	Optimised Net Thickness (mm)	Cargo Hold Actual Weight (Tonnes)	Cargo Hold Optimised Weight (Tonnes)	Initial Production Costs (€)	Optimised Production Costs (€)
Keel Plate	11.5	10.0				
Bottom Plate	9.5	8.5				
Side Shell Plate	8.5	7.5				
Shear Strake Plate	10.5	9.0				
Main Deck Plate	13.5	11.0				
DB Longitudinal Girder, CL	16.0	19.0				
Inner Side Shell Plate-1	12.5	8.5				
Inner Side Shell Plate-2	7.5	8.5	639.50	573.35	1,971,315.00	1,770,000.00
Inner Side Shell Plate-3	10.5	8.5				
Inner Bottom Plate-1	13.5	11.5				
Inner Bottom Plate-2	10.0	11.5				
Hatch Coaming Plate	14.0	12.5				
Hatch Coaming Top Plate	21.0	19.5				
Web Frame Spacing	1430.0	1484.0				
Stiffener Spacing	631.0	648.0				

Figure 20 illustrates the midship section of a multipurpose cargo ship following an optimisation process. The scantling has been optimised in this new midship section design, focusing on gross plate thickness. The gross plate thickness in the figure indicates that it represents the total thickness of structural plates and frames.

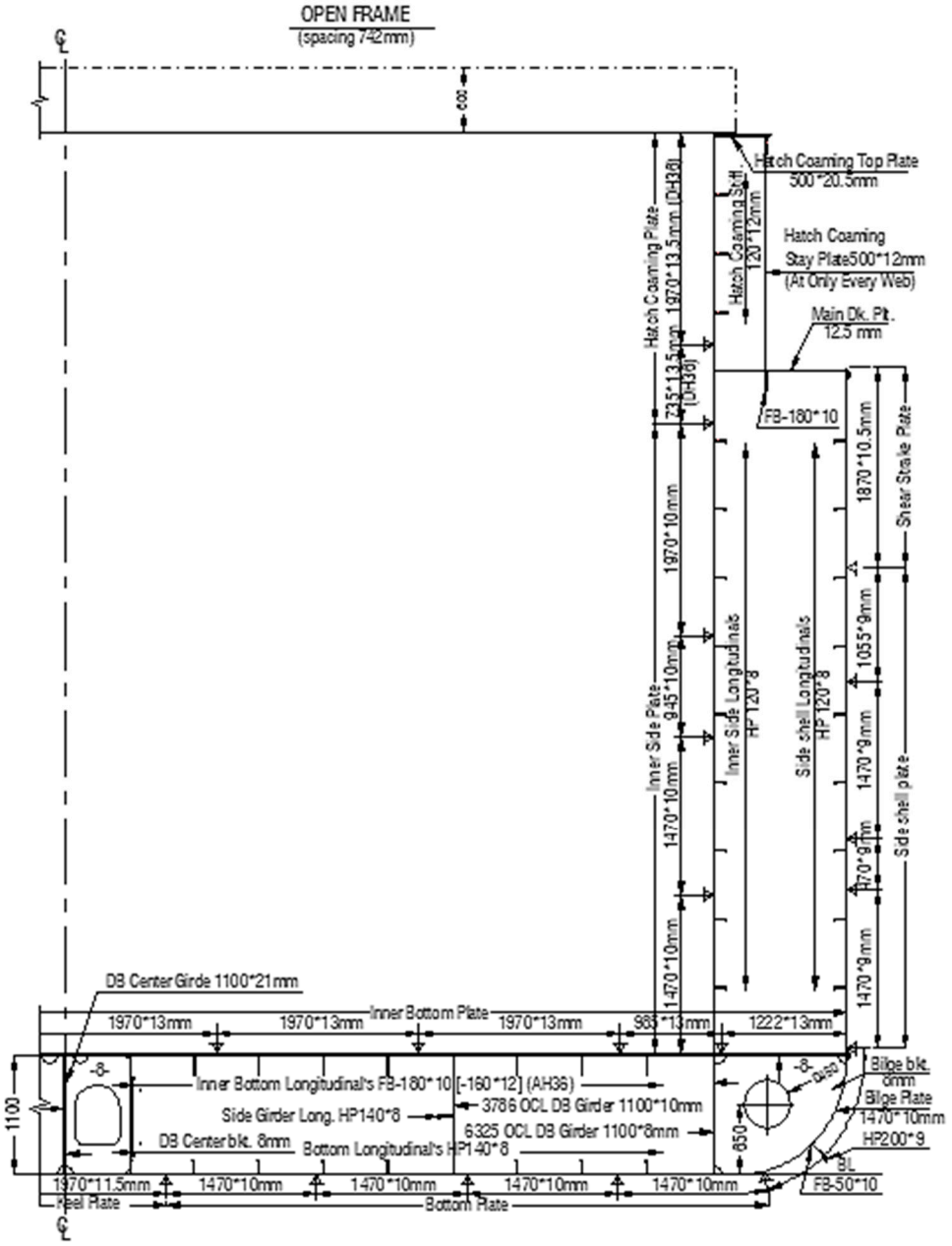

Figure 20. Midship section of the investigated ship after optimisation.

Figure 21 depicts the von Mises stress distribution along the ship's hull girder at the midship section during the sagging (upright) condition following optimisation. A significant increase in von Mises stress is evident, rising from 266.09 MPa (Figure 4) to 296.2 MPa after optimisation. This remarkable stress variation results from deliberate changes made during the optimisation process, specifically in plate thickness and the reconfiguration of web frame and stiffener spacing.

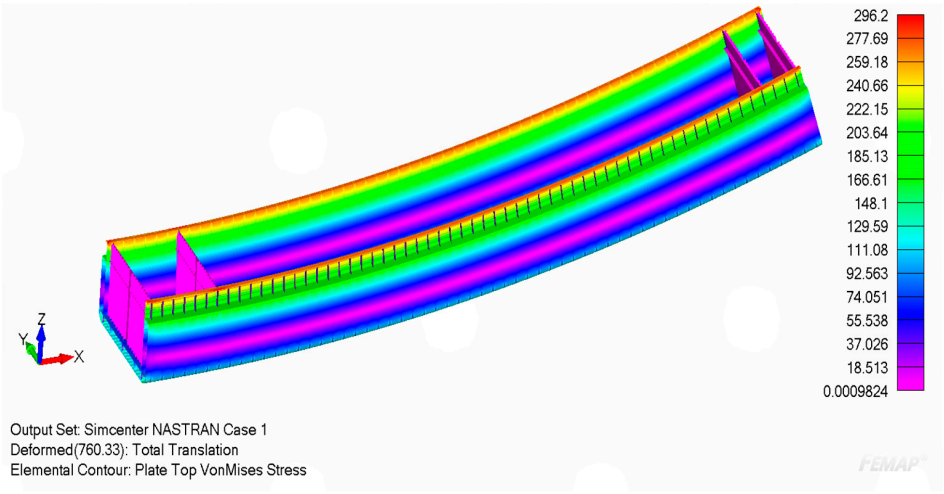

Figure 21. After optimisation, hull girder von Mises stress (MPa) at midship (sagging—upright condition).

In Figure 22, the von Mises stress in the ship's keel plate was registered at 112.04 MPa before optimisation and increased to 135.57 MPa after optimisation. Nevertheless, it is crucial to highlight that even after optimisation, these stress levels consistently remained beneath the master allowable stress limit of 219.42 MPa prescribed for grade-A steel. This demonstrates a safety factor of approximately 1.62, indicating the keel plate's structural integrity has been upheld within safe operational parameters.

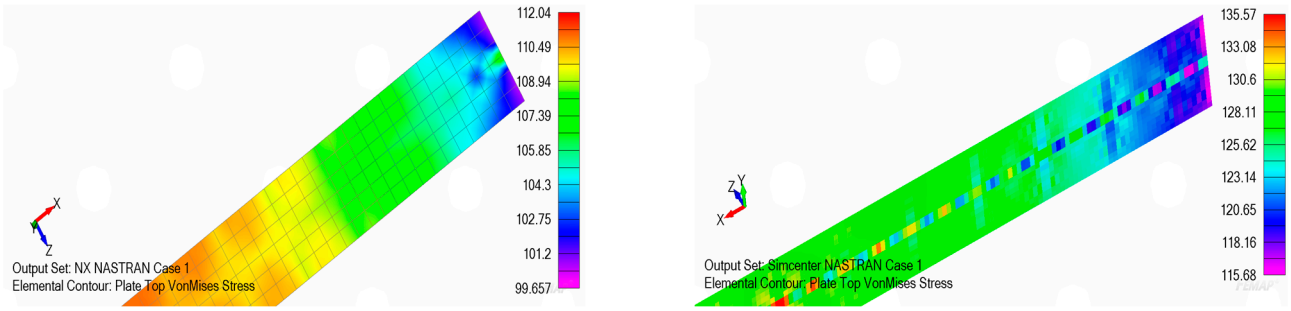

Before optimisation After optimisation

Figure 22. Keel plate von Mises stress (MPa).

Figure 23 exhibits the von Mises stress distribution in the ship's bottom plate, measuring 125.44 MPa before and 158.8 MPa after optimisation. It is imperative to underscore that these stress levels consistently reside within a safe operational range despite the enhanced stress levels post-optimisation. The master allowable stress limit, set at 219.42 MPa for grade-A steel, remains unbreached, resulting in a safety factor of approximately 1.38.

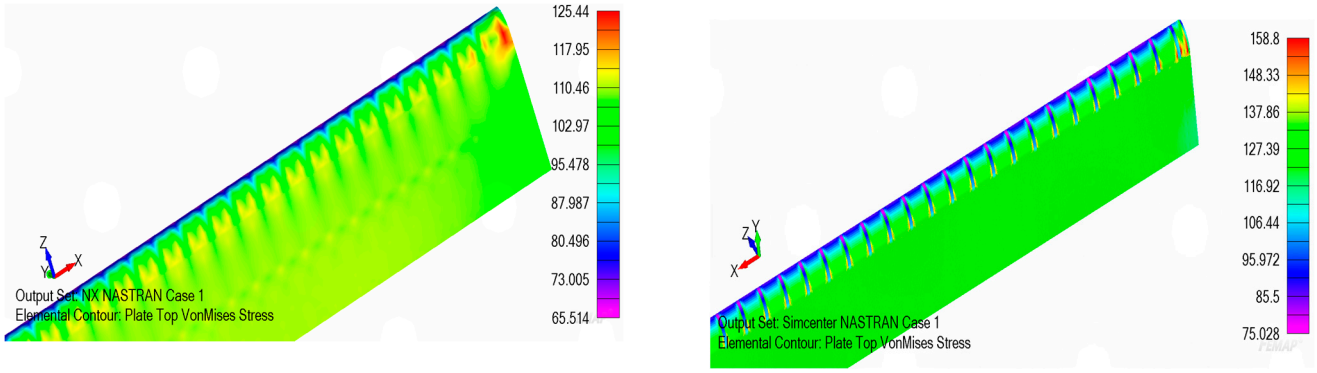

Before optimisation After optimisation

Figure 23. Bottom plate von Mises stress (MPa).

Figure 24 presents the von Mises stress distribution in the ship's side shell plate, exhibiting values of 90.64 MPa before optimisation and 111.52 MPa after optimisation. Notably, post-optimisation stress levels consistently remain significantly below the stringent master allowable stress limit of 219.42 MPa, designed for grade-A steel, resulting in a safety factor 1.97.

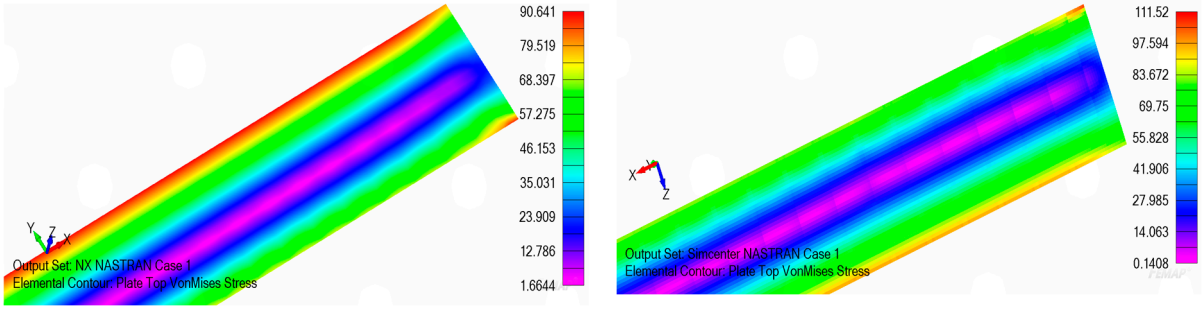

Before optimisation After optimisation

Figure 24. Side shell plate von Mises stress (MPa).

Figure 25 visually represents the von Mises stress distribution of the analysed ship's inner side shell plate. The pre-optimisation stress value was 136.82 MPa, which increased to 149.26 MPa post-optimisation. Despite the reduction in plate thickness and the consequent rise in stress concentration following optimisation, the von Mises stress in the optimised inner side shell plate comfortably remains below the defined allowable stress limit of 219.42 MPa for grade-A steel, yielding a safety factor of approximately 1.47.

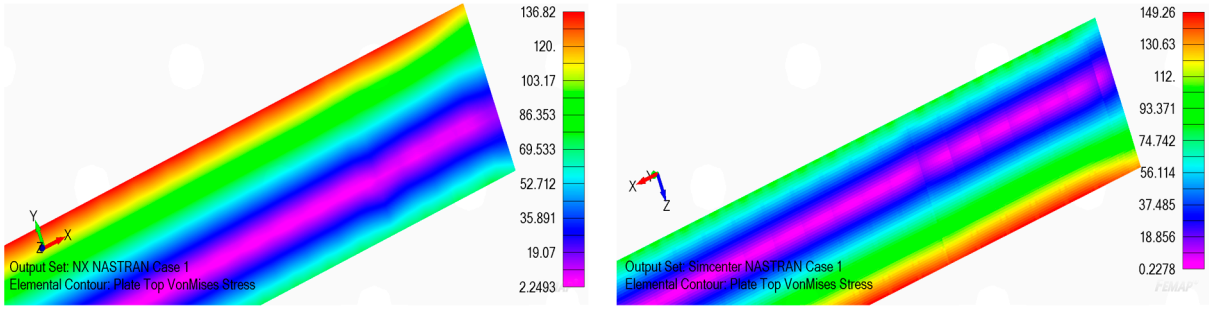

Before optimisation After optimisation

Figure 25. Inner side shell plate von Mises stress (MPa).

Figure 26 depicts the von Mises stress distribution in the analysed ship's inner bottom plate, measuring 96.41 MPa before and 128.44 MPa after optimisation. These stress values consistently remain below the allowable stress limit of 219.42 MPa designated for grade-A steel, resulting in a safety factor of approximately 1.71.

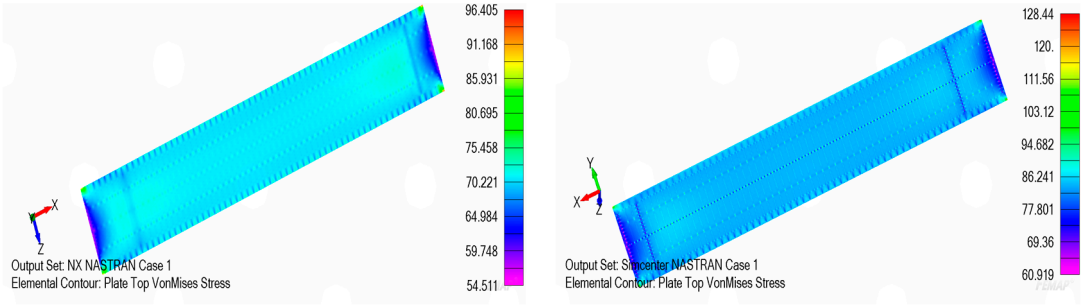

Before optimisation After optimisation

Figure 26. Inner bottom plate von Mises stress (MPa).

Figure 27 illustrates the von Mises stress distribution in the analysed ship's shear strake plate. Following a reduction in plate thickness, the stress level increased to 222.04 MPa after optimisation, compared to the pre-optimisation value of 171.55 MPa. It is noteworthy that even after optimisation, the von Mises stress remains below the allowable stress threshold of 331.77 MPa, as specified for high-tensile steel (Grade AH-36), resulting in a safety factor of approximately 1.49.

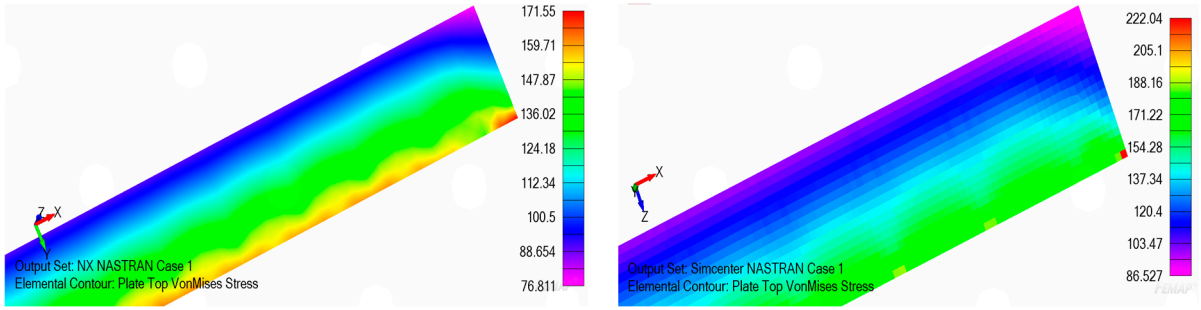

Before optimisation After optimisation

Figure 27. Shear strake plate von Mises stress (MPa).

Figure 28 depicts the von Mises stress distribution on the analysed ship's main deck. Notably, the von Mises stress in the optimised state reached 223.26 MPa, as opposed to the pre-optimisation value of 171.74 MPa. Despite this increase in stress due to the thickness reduction of the main deck, the von Mises stress consistently remains below the allowable stress threshold of 331.77 MPa for high-tensile steel (Grade AH36), resulting in a safety factor of approximately 1.49.

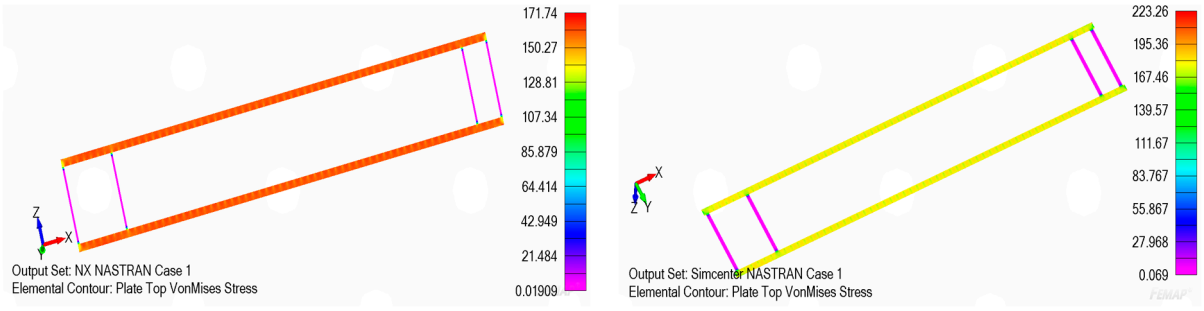

Before optimisation After optimisation

Figure 28. Main deck plate von Mises stress (MPa).

Figure 29 presents the von Mises stress distribution within the analysed ship's DB longitudinal girder, specifically the CL (centre line) section. The von Mises stress was measured at 213.35 MPa before optimisation, but an increase in plate thickness decreased to 190.51 MPa post-optimisation. This comfortably remains well below the allowable stress threshold of 219.42 MPa, as specified for Mild steel (Grade A), resulting in a safety factor of approximately 1.15.

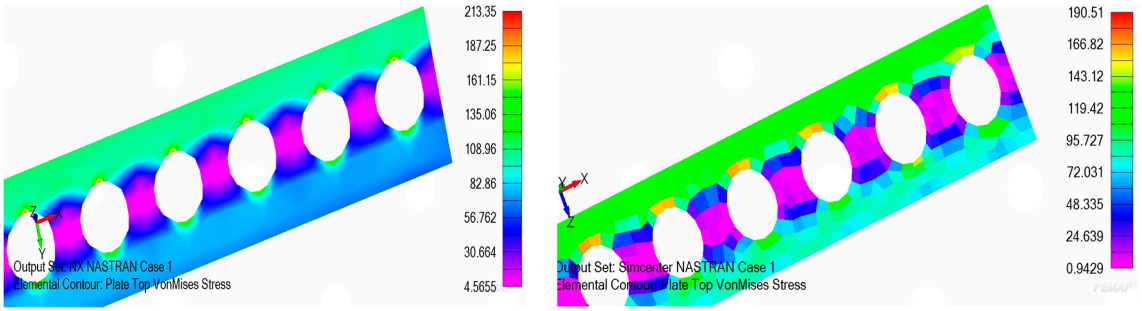

Before optimisation After optimisation

Figure 29. DB longitudinal girder, CL von Mises stress (MPa).

Figure 30 illustrates the distribution of von Mises stress within the hatch coaming plate of the analysed vessel. The von Mises stress increased from 266.09 MPa to 296.20 MPa in the optimised state compared to its initial condition. While this increase in von Mises stress is notable post-optimisation, it remains below the allowable stress threshold of 331.77 MPa, as specified for high-tensile steel (Grade DH36). This result yields a safety factor of approximately 1.12, affirming the sturdy structural integrity of the optimised hatch coaming plate.

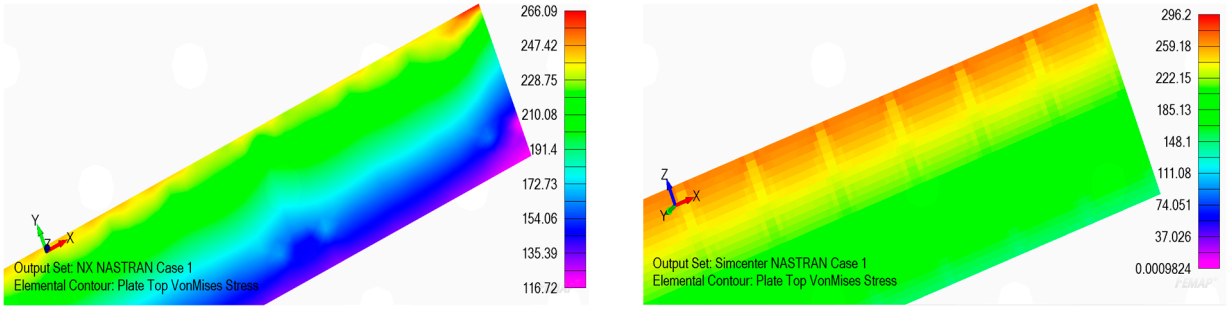

Before optimisation After optimisation

Figure 30. Hatch coaming plate von Mises stress (MPa).

Figure 31 depicts the von Mises stress distribution within the hatch-coaming top plate of the analysed vessel. Post-optimisation, the von Mises stress increased to 296.20 MPa from its pre-optimisation level of 265.23 MPa. While this notable increase in von Mises stress accompanies the reduction in plate thickness during optimisation, it consistently remains below the allowable stress threshold of 331.77 MPa, as specified for high-tensile steel (Grade DH36). This result yields a safety factor of approximately 1.12, affirming the robust structural integrity of the optimised hatch coaming top plate. Table 5 exhibits the summary of Von Mises stress before and after the optimisation of the ship.

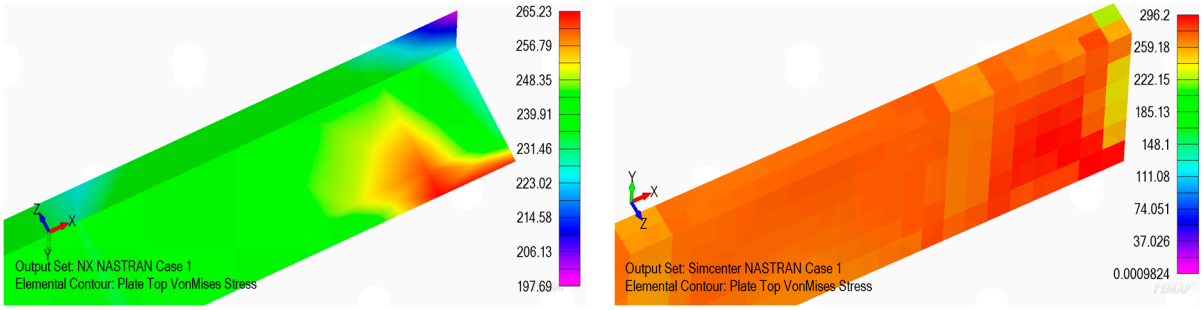

Before optimisation After optimisation

Figure 31. Hatch coaming top plate von Mises stress (MPa).

Table 7 briefly compares von Mises stress factors before and after optimisation, alongside allowable stress thresholds. It provides a comprehensive overview of critical ship components, presenting initial stress levels as a baseline, post-optimisation stress values, and acceptable stress limits by industry standards.

Table 7. Von Mises stress before and after optimisation.

Sl No.	Description	Von Mises Stress before Optimisation (MPa)	Von Mises Stress after Optimisation (MPa)	Allowable Stress (MPa)
1	Keel Plate	112.04	135.57	219.42
2	Bottom Plate	125.44	158.8	219.42
3	Side Shell Plate	90.64	111.52	219.42
4	Shear Strake Plate	171.55	222.04	331.77
5	Main Deck Plate	171.74	223.26	331.77
6	DB Longitudinal Girder	213.35	190.51	219.42
7	Inner Side Shell Plate	136.82	149.26	219.42
8	Inner Bottom Plate	96.41	128.44	219.42
9	Hatch Coaming Plate	266.09	296.20	331.77
10	Hatch Coaming Top Plate	265.23	296.20	331.77

Optimising ship structures is essential in the maritime sector to improve performance and efficiency [31]. By validating the optimised design, potential issues can be detected and resolved early on, leading to a more economically efficient and reliable final product [32].

9.1. Validation of the Optimised Midship Section

The validation of the structural integrity for the optimised midship section was meticulously conducted utilising the BV Mars 2000 software in strict adherence to the rigorous BV class rules and regulations. It is well acknowledged that the restrictions set forth by classification societies tend to lean toward conservatism. Consequently, when a validation process aligns with these rule-based regulations, it can be reasonably inferred that it will also meet the criteria set by finite element analysis. The design of the midship section of the multi-purpose vessel adheres meticulously to the standards and guidelines specified by the Classification Society.

Figures 32–34 depict the local sea loads exerted on the hull, serving to validate the optimised model. Figure 35 illustrates the cargo load acting on the vessel's inner bottom and inner side shell. The scantlings of the optimised model are determined by integrating these local sea loads and cargo loads with global hull girder loads. Local sea loads encompass hydrostatic pressure, hydrodynamic pressure, exposed deck pressure, and weather pressure. Figures 32–34 reveal that local sea loads are higher in the oblique sea than in the head and Beam Sea. Figure 36 illustrates the torsional load exerted on the hull girder. It is assumed there will be no cargo movement during sailing, so no still water torsional moment is considered. These torsional moments serve to validate the scantlings of the optimised model.

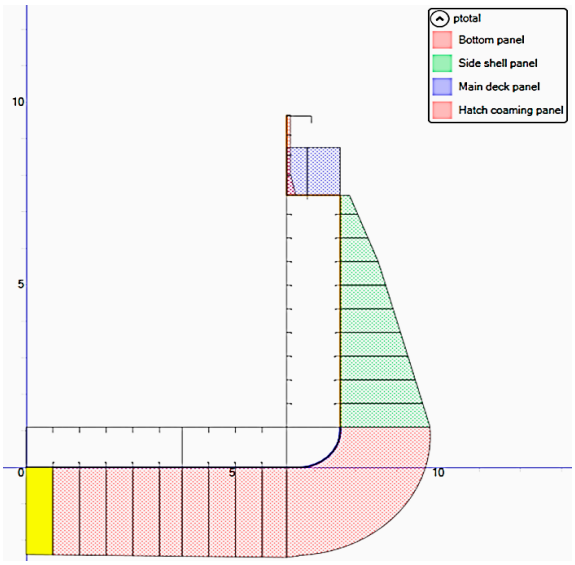

Figure 32. Local sea loads acting on the hull (Head Sea).

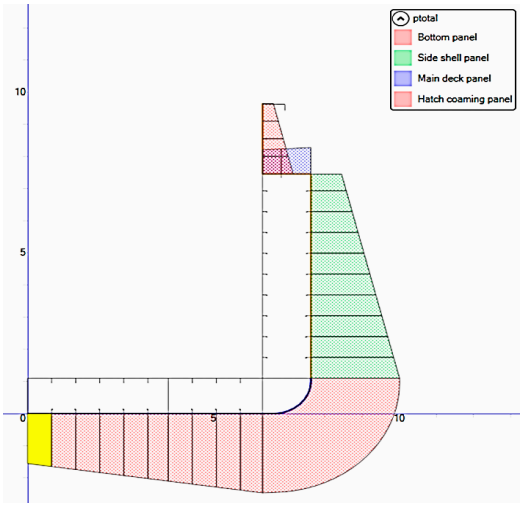

Figure 33. Local sea loads acting on the hull (Beam Sea).

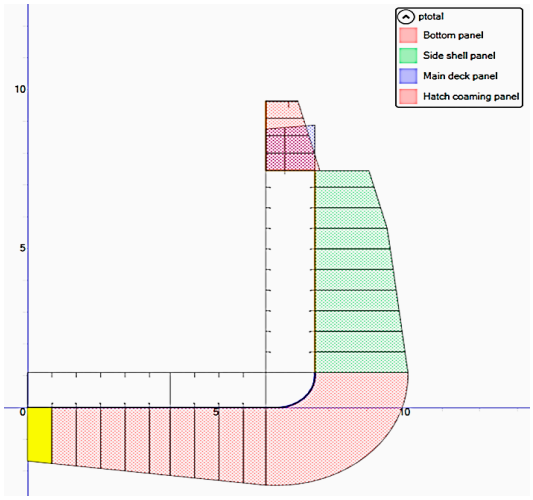

Figure 34. Local sea loads acting on the hull (Oblique Sea).

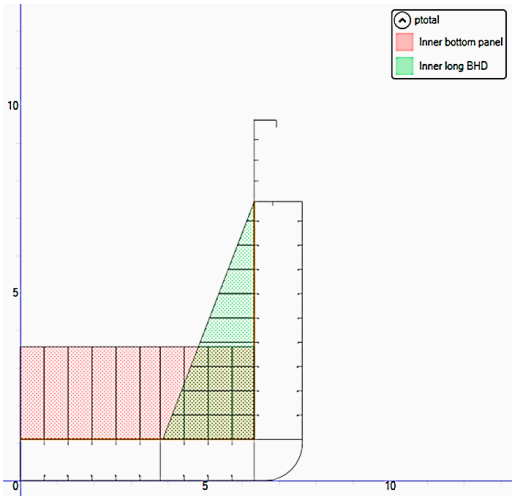

Figure 35. Cargo loads acting on the inner bottom and inner side shell.

Equivalent Design Wave	OHM		
	Dynamic Load Case		
	OHM1-S/2-P	OHM2-S/1-P	
Loads inducing torsion			
Torsion Moment (S.W.)	0	0	kN.m
Torsion moment (Wave)	-3 880	3 880	kN.m
Horizontal shear force (wave)	455	-455	kN
Torsion model results			
Torque due to Saint Venant	-471	471	kN.m
Torque due to Warping	-3 409	3 409	kN.m
Total Torque	-3 880	3 880	kN.m
Bimoment	-334 666	334 666	kN.m²

Figure 36. Torsional load acting on hull girder.

Figures 37 and 38 present an optimised midship's yielding and buckling criteria, revealing that the inner bottom plate (bottom plate one and bottom plate 2) and the double bottom side girder plate do not meet the class rule yielding criteria. At the same time, the double bottom side girder plate also fails to satisfy the class rule buckling criteria. To address these shortcomings, the inner bottom plate material grade has been upgraded from mild steel (Grade A) to higher tensile steel (Grade AH36), and an additional stiffener has been incorporated into the double bottom side girder. Subsequently, a sensitivity analysis was conducted using BV Mars 2000 software to assess further and validate the optimised midship's compliance with yielding, buckling, and ultimate hull girder strength criteria, ensuring alignment with industry standards and classification society regulations.

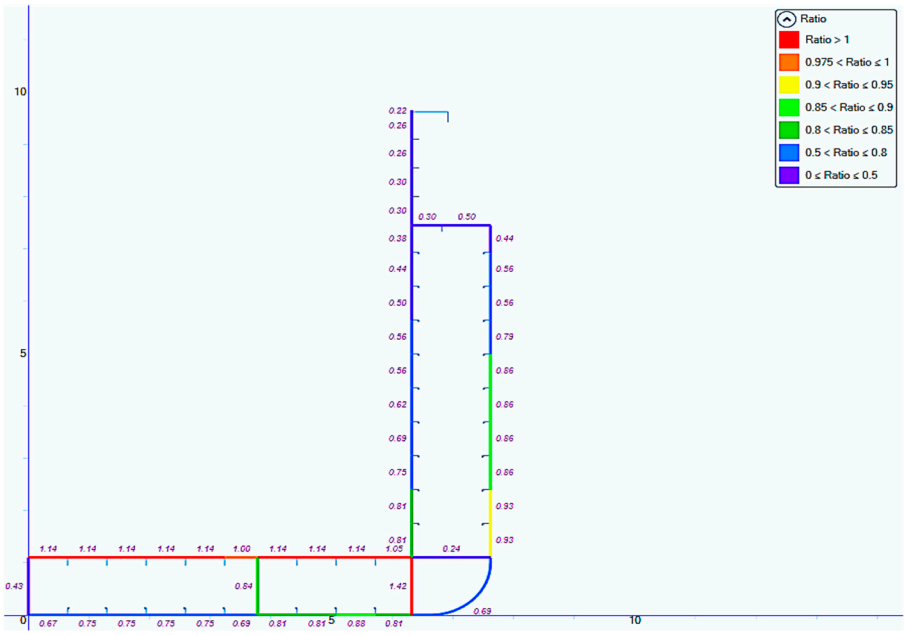

Figure 37. Yielding criteria of the optimised midship.

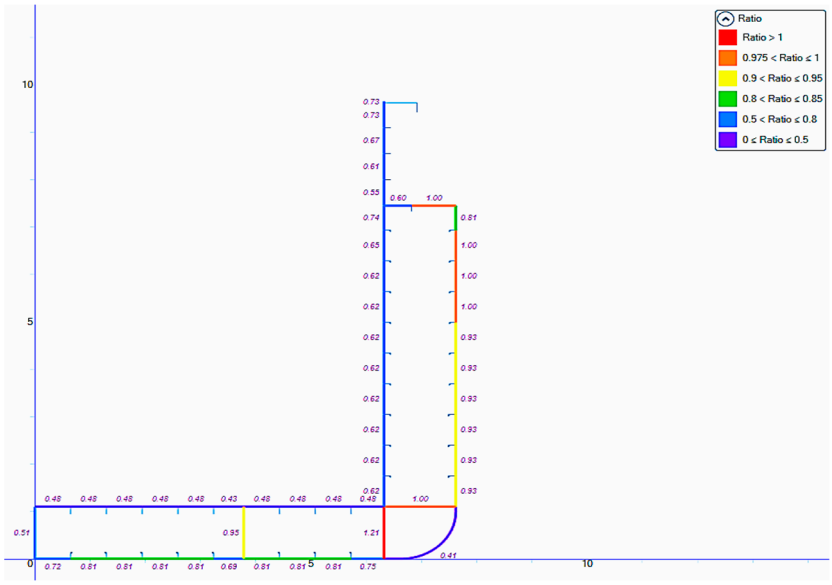

Figure 38. Buckling criteria of the optimised midship.

9.2. Yielding Assessment

The validation process for the optimised midship section is crucial for marine vessels, encompassing evaluations to ensure structural integrity and functionality. It involves the application of principles and methodologies to assess the midship section's ability to withstand yielding and adhere to permissible stress conditions, including its response to hull girder bending, shear forces, and the risk of yielding-induced failure. Understanding the midship section's limits and capacity to handle various loads is essential for designing safe and reliable vessels. The outcomes of this assessment inform critical decisions regarding the midship section's design, material selection, and reinforcement strategies [33].

Figures 39 and 40 demonstrate that the utilisation factor about the hull girder bending strength of the plating remains consistently below one for both head sea and oblique sea conditions, thus effectively meeting the stipulated rule criteria. This analysis found that head sea conditions are the most challenging, with the highest hull girder bending stress occurring near the hatch coaming area.

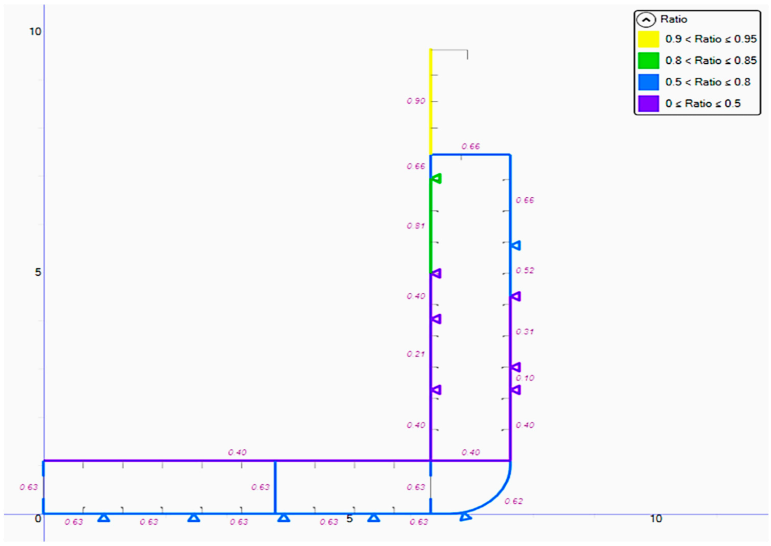

Figure 39. Validation of hull girder bending strength for plating (Head Sea).

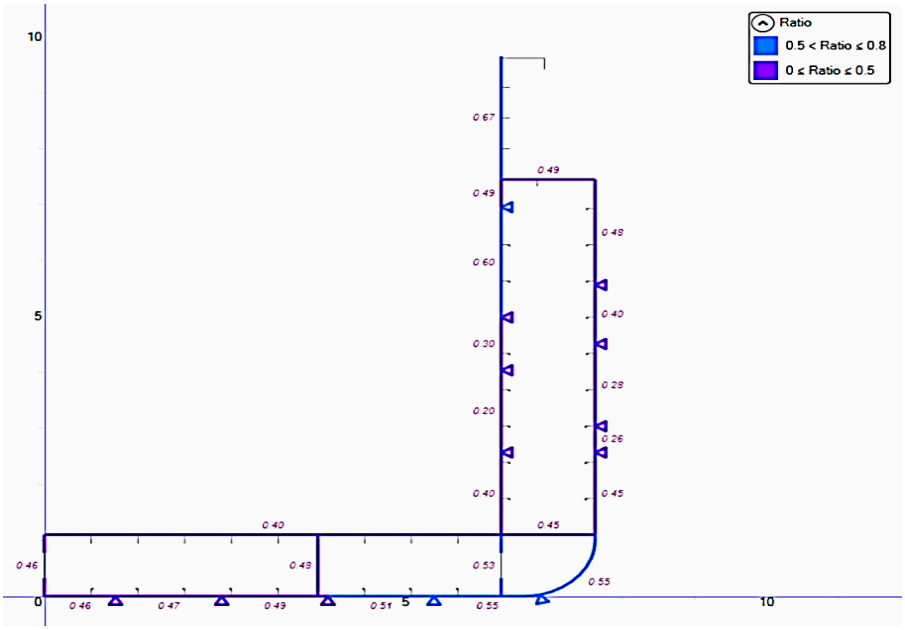

Figure 40. Validation of hull girder bending strength for plating (Oblique Sea).

Figures 41 and 42 indicate that the utilisation factor of an ordinary stiffener's hull girder strength consistently remains below 1, which complies with established rule criteria for both head sea and oblique sea scenarios. The head sea condition is the most challenging, with the highest hull girder stress concentration at the hatch coaming area.

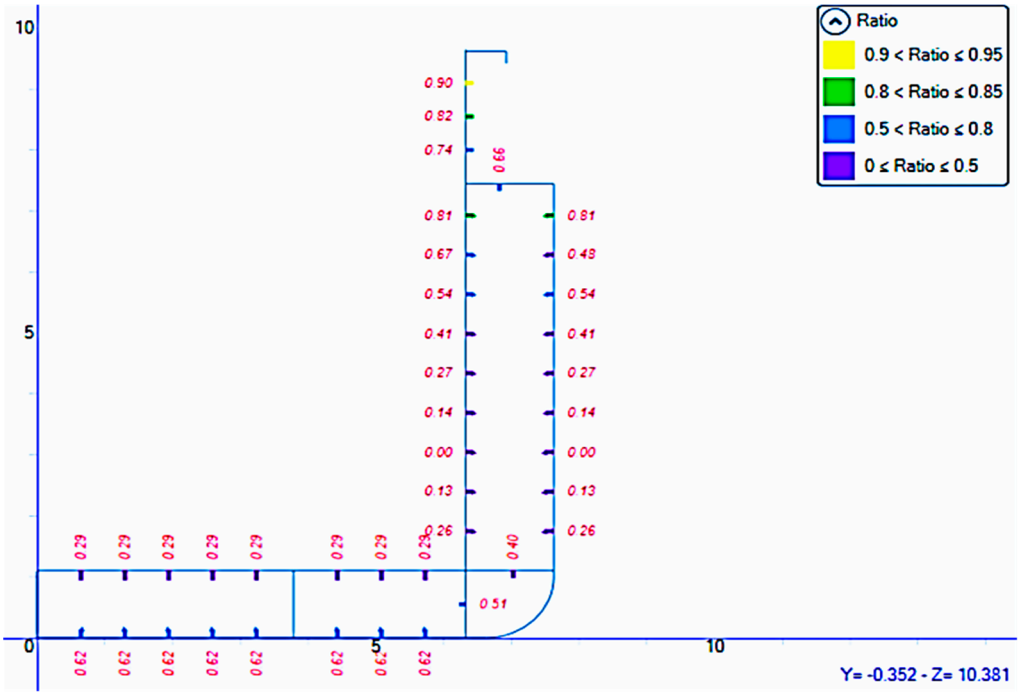

Figure 41. Validation of hull girder strength for ordinary stiffener (Head Sea).

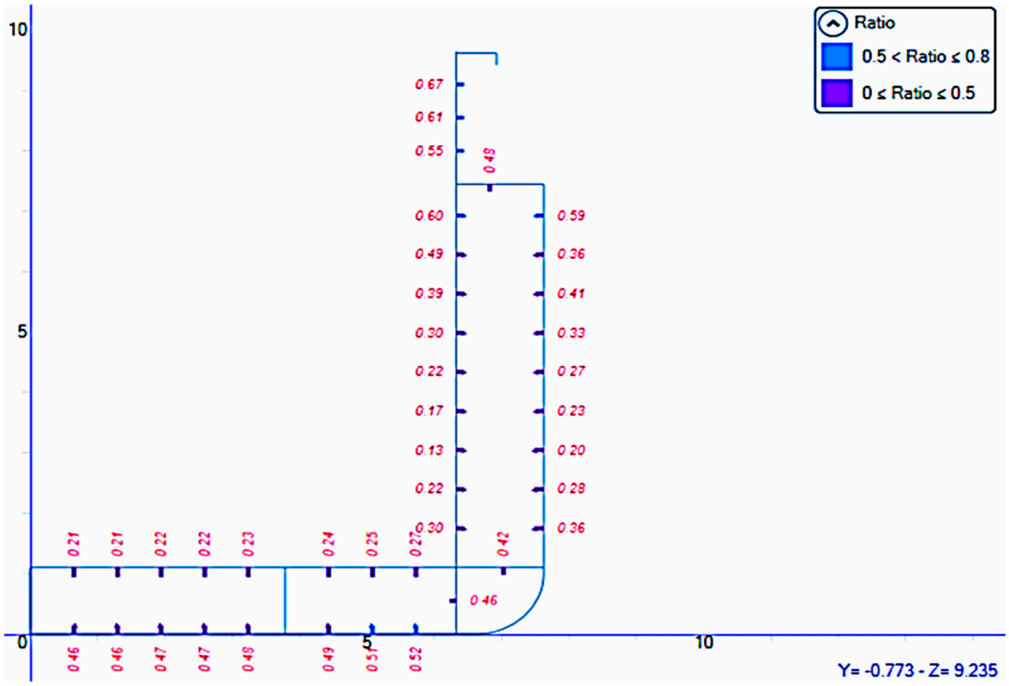

Figure 42. Validation of hull girder strength for ordinary stiffener (Oblique Sea).

Figures 43 and 44 show that the utilisation factor about the shear strength of plating in the hull girder consistently remains below 1. This indicates that the vessel complies with the established rule criteria, regardless of whether it encounters head or oblique sea conditions. It is worth noting that the area with the highest hull girder shear stress is located near the neutral axis, which confirms the findings of previous studies regarding the ultimate strength of ship hull girders. This emphasises the significant role of shear strength in maintaining structural resilience in maritime vessels. Furthermore, Figure 45 provides a graphical representation of the primary vertical distribution of hull girder shear stress, which offers valuable insights into the subtle stress patterns within the hull girder structure.

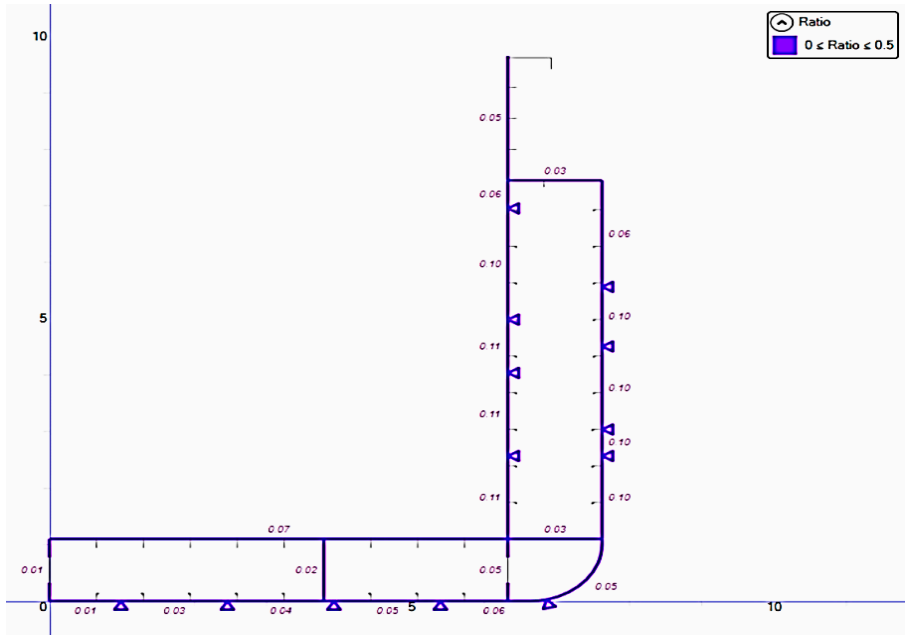

Figure 43. Validation of hull girder shear strength for plating (Head Sea).

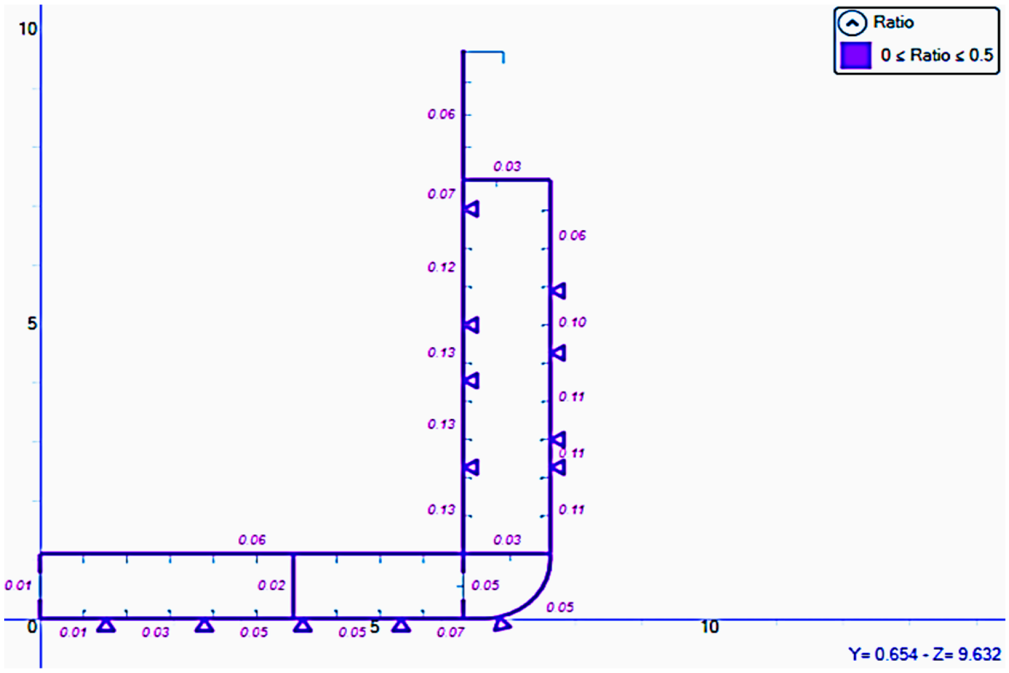

Figure 44. Validation of hull girder shear strength for plating (Oblique Sea).

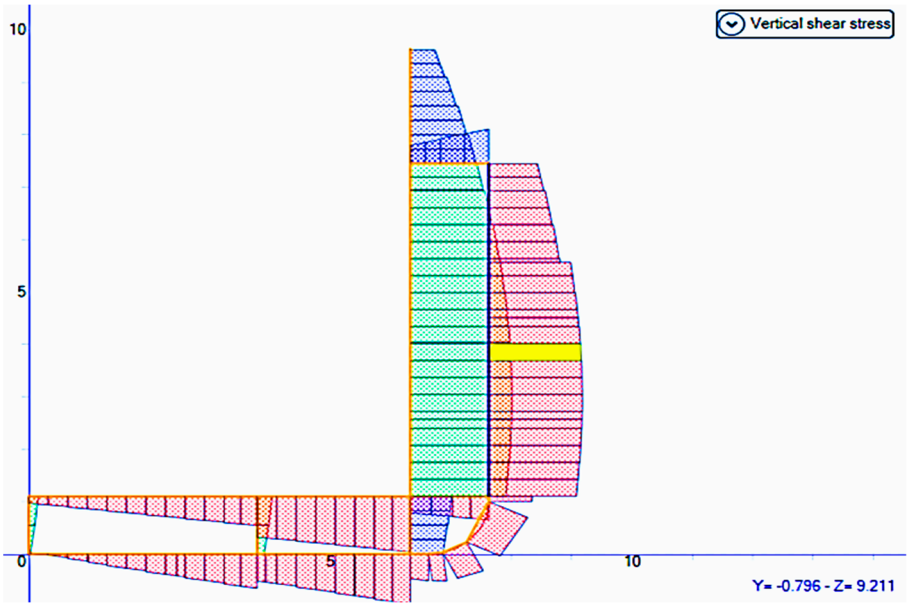

Figure 45. Primary vertical hull girder shear stress distribution.

9.3. Buckling Assessment

The validation of an optimised midship section necessitates a fundamental buckling assessment, a cornerstone of ship design. This assessment thoroughly evaluates the midship section's structural stability when subjected to compressive loads, ensuring its resilience against buckling phenomena. Notably, the study employed Bureau Veritas software, MARS 2000, to conduct an in-depth analysis of the hull girder's buckling behaviour, highlighting the critical importance of leveraging numerical tools in such assessments [34].

Figure 46 illustrates the buckling capacity of plate panels within the optimised midship section, adhering to BV (Bureau Veritas) rules. A critical factor is that a buckling factor exceeding 1 indicates a failure to meet the buckling criteria. All plate panels exhibit utilisation factors below 1, demonstrating full compliance with the stipulated rule criteria.

The investigation into weight and cost optimisation of the midship section, aligning with standard structural regulations, reaffirms the observed increase in plate buckling within the optimal solution.

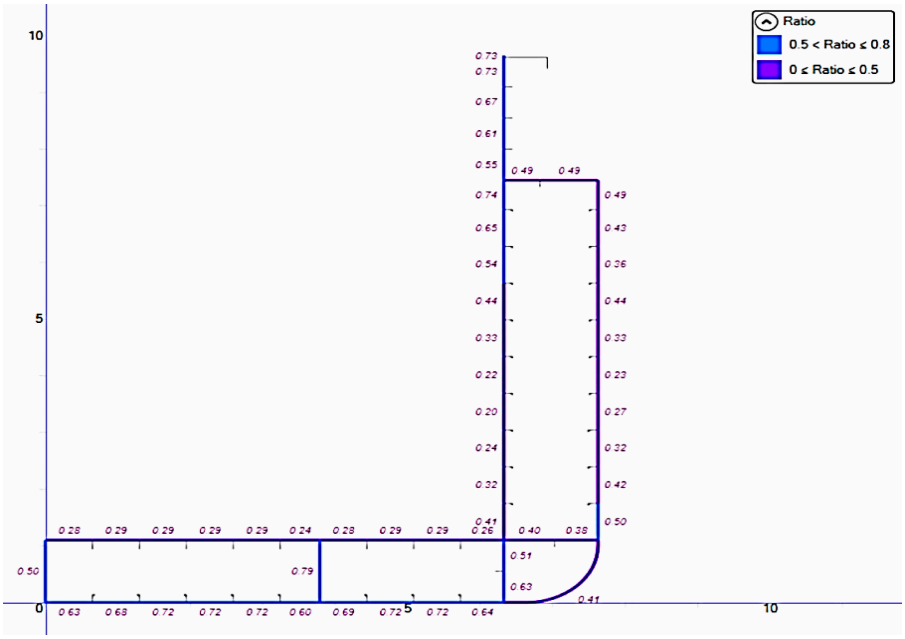

Figure 46. Validation of buckling of plate panel.

In Figure 47, the buckling utilisation factor for ordinary stiffeners is consistently less than one, aligning with the general methods for determining buckling capacities of plate panels, stiffeners, primary supporting members, and columns as specified in the applicable rules. This utilisation factor is a crucial parameter in evaluating the structural integrity of stiffened panels, with the requirement that it remains below 1 to meet the rule criteria.

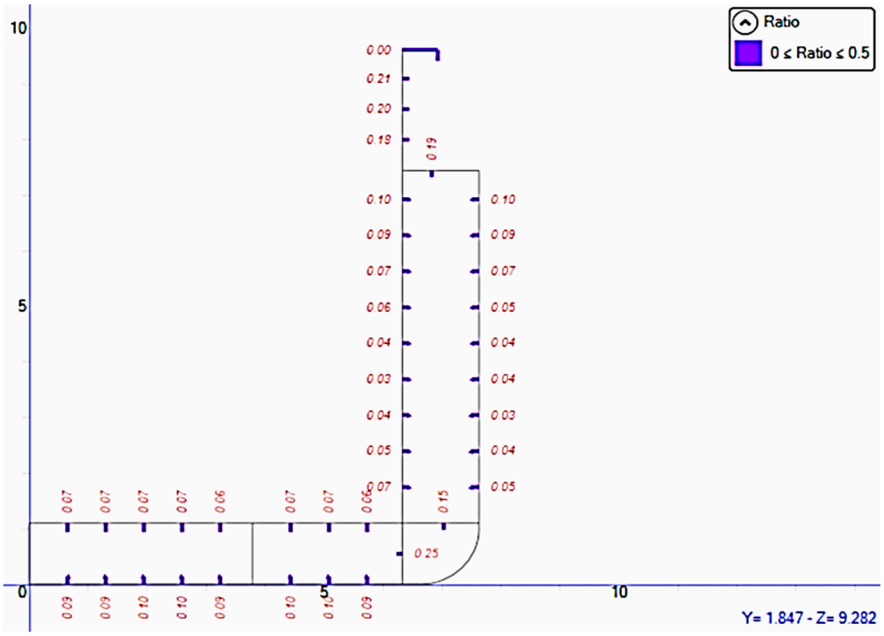

Figure 47. Validation of buckling of ordinary stiffener.

9.4. Ultimate Strength Assessment

The assessment of a ship's hull girder's ultimate strength holds paramount importance in ensuring the structural integrity of a vessel, incredibly when validating an optimised midship section. The hull girder's ultimate strength (HGUS) signifies the maximum bending capacity the hull girder can withstand when exposed to longitudinal pressure, a crucial factor in ensuring the vessel's safety [35]. To conduct this assessment, Bureau Veritas software, MARS 2000, was employed, utilising the progressive collapse method to examine the ultimate strength of the hull girder within the space delineated by two adjacent frames.

The simplified progressive collapse method relies on several key assumptions [36]:

1. Simple beam assumption: This assumption suggests that the cross-section remains plain throughout the progressive collapse process, with deviations occurring only when substantial deflection and local deformation are induced.
2. Independency assumption: According to this assumption, there is no interaction or influence between adjacent elements during the collapse. It holds well when the cross-section experiences predominantly vertical bending.
3. Interframe collapse assumption: This assumption assumes that transverse frames possess sufficient strength, resulting in all elements failing in an inter-frame mode.

Notably, as illustrated in Figure 48, the ultimate strength is highest under hogging loading conditions and lowest under sagging loading conditions. The most critical structural failure scenario arises in sagging loading conditions, representing the most challenging condition for ensuring structural integrity.

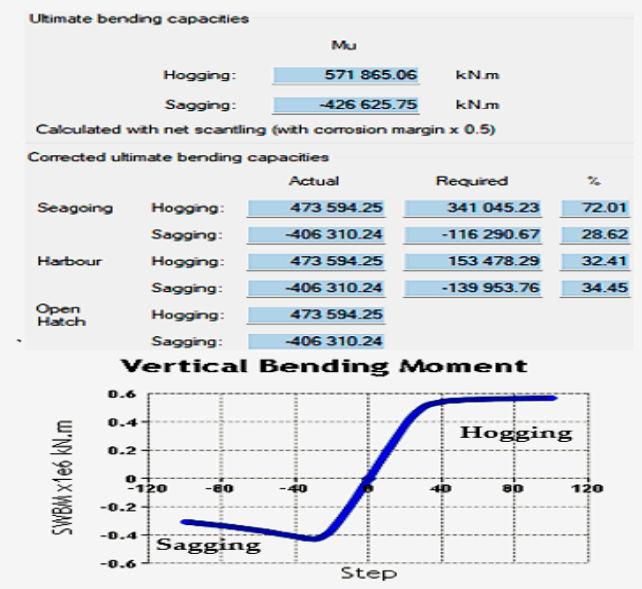

Figure 48. Hull girder's ultimate strength.

Figure 48 indicates that a modification in ultimate strength can be most efficiently accomplished by adjusting the thickness of structural components [37]. This adjustment involves maintaining the thickness of the structure nearest to the neutral axis constant (including the inner side and side shell) while varying the thickness of the structure located farthest from the neutral axis (such as the bottom, double bottom, and deck structure), where global failure is most likely to occur. The ultimate strength of a material is the maximum stress it can withstand before breaking.

10. Discussion

The study used the Design of Experiment (DOE) methodology with a fractional factorial design technique to create regression equations for von Mises stress and production

costs in multipurpose cargo ship design. This comprehensive approach involved analysing twelve significant structural components of the ship using Minitab software, examining 128 diverse models. The derived regression equations were subsequently incorporated into a Python-based, Non-dominated Sorting Genetic Algorithm II (NSGA-II) to optimise the multipurpose cargo ship's weight and production costs. Fractional factorial designs are a valuable alternative to full factorial designs as they require fewer experimental runs and prove incredibly beneficial when resources are constrained. These designs offer multiple advantages, including economic efficiency achieved by reducing the number of experimental runs. Additionally, they provide a more focused and pertinent approach, enabling the prioritisation of the most impactful factors and effects. This prioritisation is crucial for ensuring the structural integrity and cost-effectiveness of the ships.

Preserving a ship's structural integrity is paramount to ensure both its crew's and the ship's safety, especially in demanding marine environments characterised by saltwater exposure and strong waves. This study focuses on maintaining von Mises stress levels within critical locations well below permitted stress thresholds. For mild steel (Grade A) and high-tensile steel (Grade AH36 and Grade DH36), the maximum permissible stress thresholds are 219.42 MPa and 331.77 MPa, respectively (see Section 2.1). Figures 20 and 21 illustrate the midship section of the optimised ship and its analysed cargo hold model in a sagging condition, demonstrating compliance with these permitted stress thresholds. Figures 27, 28, 31 and 32 provide further evidence, revealing that the von Mises stress levels of the Shear strake plate (Grade AH36), Main Deck plate (Grade AH36), Hatch Coaming plate (Grade DH36), and Hatch Coaming top plate (Grade DH36) remain comfortably below permitted stress thresholds after optimisation, with values of 222.04 MPa, 223.26 MPa, 296.20 MPa, and 296.2 MPa, respectively.

Additionally, Figures 22–26 and 29 present von Mises stress distributions across various critical ship components, including the Keel plate (Grade A), Bottom plate (Grade A), Side Shell plate (Grade A), Inner Side Shell plate (Grade A), Inner Bottom plate (Grade A), and double bottom longitudinal girder, CL (Grade A), which offer valuable insights into the structural integrity and performance of these components under different loading conditions and provide essential data for assessing their reliability and safety during operational scenarios. In all cases, stress levels consistently remain significantly lower than permitted stress thresholds, with values of 135.57 MPa, 158.80 MPa, 111.52 MPa, 149.26 MPa, 128.44 MPa, and 190.51 MPa, respectively. Notably, the von Mises stress of the double bottom longitudinal girder, CL (Grade A), decreased from 213.35 MPa before optimisation to 190.51 MPa after optimisation, ensuring ample safety factors. These findings emphasise the vital role of structural optimisation in enhancing ship safety and performance in challenging maritime conditions. Adjustments were made to the main frame spacing, web frame spacing, and the repositioning of longitudinal stiffeners, all accomplished without modifying the ship's fundamental dimensions to optimise the cargo hold region.

Strict adherence to time-honoured industry practices and classification society standards is imperative in shipbuilding. Key among these principles is the hierarchy of structural plate thickness, with stipulations that the Keel plate should possess a thickness greater than or equal to the Bottom plate, the Bottom plate thickness should exceed or be similar to that of the Side shell plate, and the Shear strake plate thickness should be greater than or equal to the Side shell plate thickness. In this extensive study, meticulous validation and maintenance of these established relationships are evident, as in Table 4. This adherence reaffirms the enduring relevance of these traditional practices and underscores their indispensable role in contemporary ship design. Upholding these thickness hierarchies enhances the overall safety, reliability, and performance of ships, ensuring their suitability for challenging maritime conditions and reinforcing the pivotal role of industry conventions in modern shipbuilding.

After optimisation, a novel midship section featuring modified scantlings has been meticulously designed for the analysed ship. This midship section has undergone a

comprehensive validation process. Figures 31 and 32 visually represent the optimised midship's yielding and buckling criteria, clearly depicting the local strength criteria of plates and ordinary stiffeners, such as yielding and buckling, revealing that the inner bottom plates (bottom plate one and bottom plate two) and the double bottom side girder plate do not adhere to the class rule yielding criteria. The double bottom side girder plate also fails to meet the class rule buckling criteria. To rectify these deficiencies, the material grade of the inner bottom plate has been upgraded from mild steel (Grade A) to higher tensile steel (Grade AH36), and an additional stiffener has been integrated into the double bottom side girder. Subsequently, a sensitivity analysis was conducted using BV Mars 2000 software to assess further and validate the optimised midship's compliance with yielding (See Figures 39–44), buckling (See Figures 46 and 47), and ultimate hull girder strength (See Figure 48) criteria, ensuring alignment with industry standards and classification society regulations. It is noteworthy that the ship has successfully met these rigorous requirements.

The original cargo hold model weighed 639.50 tonnes before optimisation but was reduced to 573.35 tonnes after optimisation. This remarkable 66-tonne reduction significantly impacts ship performance, enhancing fuel efficiency, speed, and manoeuvrability. Additionally, it contributes to approximately 10% substantial cost reduction in building, operational, and maintenance costs. Notably, it positively impacts the environment by reducing greenhouse gas emissions and other pollutants. Concurrently, the production costs related to the ship's structure decreased from 1,971,315.00 euros to 1,770,000.00 euros after optimisation. This simultaneous 10% reduction in weight and production costs underscores the economic benefits of the optimisation process, highlighting its cost-effectiveness.

This study provides a comprehensive review of relevant literature to position its findings within the broader ship structural optimisation research landscape. For example, A.M.H. Elhewy et al. [3] optimised an offshore supply vessel (OSV) using the blind search technique, resulting in a 42% reduction in the vessel's steel weight and production cost without compromising structural integrity. Similarly, Motta et al. [12] utilised the LBR-5 programme to optimise the multi-structures of a Mega Yacht, resulting in a commendable 20% reduction in cost and an 8% reduction in weight compared to the original scantlings. These studies underscore the advantages of structural optimisation for smaller vessels. Moreover, Rigo, P. and Caprace, J.-D. [31] delved into the symbiotic relationship between "Design" and "Optimisation" in ship structures, demonstrating that optimisation efforts can yield cost savings, decreased steel usage, and enhanced performance through multi-objective optimisation techniques. These findings are consistent with the current study's findings, where structural optimisation led to a 10% reduction in steel weight and production costs while preserving the ship's principal dimensions. Furthermore, the achievement of the Pareto optimal front, as demonstrated in the work of H.Y. Alhammadi and J.A. Romagnoli [25], emphasises the significance of these findings in the context of previous research efforts. By placing these results within the broader body of work, this study highlights its relevance and substantial contribution to ship structural optimisation, underscoring its critical role in ensuring both the structural integrity and cost-effectiveness of ships in maritime engineering.

In brief, combining the fractional factorial design technique and the Python-based Non-dominated Sorting Genetic Algorithm II (NSGA-II) has proven essential in identifying and optimising the key parameters significantly influencing multipurpose cargo ship performance. The utilisation of this methodology has resulted in significant decreases in both weight and production costs while concurrently improving the overall structural robustness. This study paves the way for increased fuel efficiency, cost-effectiveness, and a more favourable environmental impact in the maritime industry by emphasising the transformative influence of ship design.

11. Conclusions

The study presented herein addressed a critical research gap in maritime engineering by focusing on the structural optimisation of a three-cargo hold model for a multipurpose

cargo ship. Significant advancements were made in enhancing ship designs' structural robustness and cost-effectiveness through the innovative integration of Design of Experiments (DOE) principles within Minitab software and utilising the Non-dominated Sorting Genetic Algorithm II (NSGA-II) managed by Python software. The following conclusions can be drawn from this research:

1. Identification of Critical Factors: The application of the fractional factorial design technique facilitated the identification of critical parameters influencing both hull girder stress and production costs in multipurpose cargo ships. This comprehensive analysis pinpointed critical structural components and design parameters, revealing the top five factors impacting hull girder stress: the Hatch coaming plate, Hatch coaming top plate, Main deck plate, Shear strake plate, and Bottom plate. Additionally, vital parameters affecting production costs were identified, including the Inner bottom plate, Inner side shell plate, Web frame spacing, and Side shell plate.
2. Efficient Optimisation Process: Integrating the NSGA-II algorithm enabled efficient optimisation of the multipurpose cargo ship's design objectives, reducing weight and production costs. Through prudent adjustments in plate thickness, web frame positioning, and stiffener arrangement, a significant 10% reduction in both ship weight and production costs was achieved, underscoring the efficacy of the optimisation process.
3. Rigorous Validation and Compliance: The optimally designed midship section underwent thorough validation to ensure conformity with industry standards and classification society regulations. Necessary adjustments were made to inner bottom plates and double bottom side girders to meet stringent requirements, emphasising the commitment to structural integrity and safety.
4. Economic and Environmental Implications: The optimisation outcomes, notably the substantial reductions in steel weight and production costs, carry significant financial implications, including enhanced economic efficiency, reduced fuel consumption, and lower initial costs. Moreover, these improvements contribute to environmental benefits by curbing greenhouse gas emissions and pollutants, aligning with sustainability goals in the maritime industry.

In summary, integrating fractional factorial design and the NSGA-II algorithm proved instrumental in optimising ship designs, resulting in tangible improvements in efficiency, cost-effectiveness, and environmental sustainability. These findings hold substantial implications for the maritime industry, paving the way for adopting more efficient and eco-friendly ship designs to meet evolving demands and challenges in marine engineering.

Author Contributions: Conceptualization, J.A., F.F. and S.M.I.M.; methodology, J.A., F.F. and S.M.I.M.; software, J.A.; validation, J.A. and F.F.; formal analysis, J.A. and S.M.I.M.; resources, J.A. and S.M.I.M.; writing—original draft preparation, J.A.; writing—review and editing, J.A., F.F. and S.M.I.M.; supervision, F.F.; project administration, J.A. and F.F. All authors have read and agreed to the published version of the manuscript.

Funding: This research received no external funding.

Institutional Review Board Statement: Not applicable.

Informed Consent Statement: Not applicable.

Data Availability Statement: The article includes the data supporting the findings and can be obtained from the corresponding authors upon request.

Acknowledgments: First and foremost, I would like to thank and convey my gratitude to Francis Franklin, my supervisor and co-author of this work, who always comes forward to assist me whenever I ask for advice on my research. Additionally, I would like to thank Bureau Veritas and Siemens Digital Industries Software for permitting me to use their software, BV Mars 2000, and Femap/Nastran, respectively.

Conflicts of Interest: The authors affirm that they do not have any known competing financial interests or personal relationships that might have influenced the work presented in this paper.

References

1. Sekulski, Z. Ship hull structural multiobjective optimization by evolutionary algorithm. *J. Ship Res.* **2014**, *58*, 45–69. [CrossRef]
2. Yu, Y.-Y.; Jin, C.-G.; Lin, Y.; Ji, Z.-S. A practical method for ship structural optimization. In Proceedings of the Twentieth International Offshore and Polar Engineering Conference, Beijing, China, 20–25 June 2010; International Society of Offshore and Polar Engineers: Houston, TX, USA, 2010.
3. Elhewy, A.M.; Hassan, A.M.; Ibrahim, M.A. Weight optimization of offshore supply vessel based on structural analysis using finite element method. *Alex. Eng. J.* **2016**, *55*, 1005–1015. [CrossRef]
4. Adarsh, M.; Anjali, A.P.; Athira, A.P.; Abhijith, A. Topology optimization of deep beam Ansys. *Int. J. Sci. Res. Rev.* **2020**, *12*.
5. Louvros, P.; Boulougouris, E.; Coraddu, A.; Vassalos, D.; Theotokatos, G. Multi-objective optimisation as an early design tool for smart ship internal arrangement. *Ships Offshore Struct.* **2022**, *17*, 1392–1402. [CrossRef]
6. Pereira, T.; Garbatov, Y. Multi-attribute decision-making ship structural design. *J. Mar. Sci. Eng.* **2022**, *10*, 1046. [CrossRef]
7. Pavlovic, A.; Sintoni, D.; Fragassa, C.; Minak, G. Multi-objective design optimization of the reinforced composite roof in a solar vehicle. *Appl. Sci.* **2020**, *10*, 2665. [CrossRef]
8. Pavlovic, A.; Fragassa, C. Geometry optimization by fem simulation of the automatic changing gear. *Rep. Mech. Eng.* **2020**, *1*, 199–205. [CrossRef]
9. Raikunen, J.; Avi, E.; Remes, H.; Romanoff, J.; Lillemäe-Avi, I.; Niemelä, A. Optimisation of passenger ship structures in concept design stage. *Ships Offshore Struct.* **2019**, *14* (Suppl. S1), 320–334. [CrossRef]
10. Andric, J.; Prebeg, P.; Zanic, V. Multi-level Pareto supported design methodology-application to RO-PAX structural design. *Mar. Struct.* **2019**, *67*, 102638. [CrossRef]
11. Ma, M.; Hughes, O.; Paik, J.K. Ultimate strength based stiffened panel design using multi-objective optimization methods and its application to ship structures. In Proceedings of the PRADS2013, CECO, Changwon City, Republic of Korea, 20–25 October 2013.
12. Motta, D.; Caprace, J.D.; Rigo, P.; Boote, D. Optimization of Hull Structures for a 60 meters Mega Yacht. In Proceedings of the 11th International Conference on Fast Sea Transportation, Honolulu, HI, USA, 26–29 September 2011.
13. Rigo, P.; Liege, U.O. An integrated software for scantling optimization and least production cost. *Ship Technol. Res.* **2003**, *50*, 125–140. [CrossRef]
14. Caprace, J.-D.; Bair, F.; Rigo, P. Scantling multi-objective optimisation of a LNG carrier. *Mar. Struct.* **2010**, *23*, 288–302. [CrossRef]
15. Ahmed, F. Development of Guidelines Allowing to Predict the Contribution of the Superstructure to the Hull Girder Strength. 2017. Available online: https://www.semanticscholar.org/paper/Development-of-guidelines-allowing-to-predict-the-Ahmed/f32e6c5e358dc129500da716f43cded60c491f5f (accessed on 21 February 2024).
16. Veritas, B. *NR 467 Rules for the Classification of Steel Ships*; Bureau Veritas Marine & Offshore: Paris, France, 2018.
17. Montgomery, D.C. *Design and Analysis of Experiments*; John Wiley & Sons: Hoboken, NJ, USA, 2017.
18. Shina, S. *Industrial Design of Experiments: A Case Study Approach for Design and Process Optimization*; Springer Nature: Berlin/Heidelberg, Germany, 2022.
19. Tyssedal, J.; Samset, O. Analysis of the 12 run Plackett-Burman design. *Prepr. Stat.* **1997**.
20. Karlapudi, A.P.; Krupanidhi, S.; Reddy, R.; Indira, M.; Md, N.B.; Venkateswarulu, T.C. Plackett-Burman design for screening of process components and their effects on production of lactase by newly isolated Bacillus sp. VUVD101 strain from Dairy effluent. *Beni-Suef Univ. J. Basic Appl. Sci.* **2018**, *7*, 543–546. [CrossRef]
21. Diewald, B.G.; Ehlers, S. On the influence of primary and secondary structural members on the global strength of ship structures. *Marit. Technol. Eng.* **2016**, *3*, 435–441.
22. Sekulski, Z. Structural weight minimization of high speed vehicle-passenger catamaran by genetic algorithm. *Pol. Marit. Res.* **2009**, *16*, 11–23. [CrossRef]
23. Caprace, J.-D.; Bair, F.; Rigo, P. Least weight and least cost optimisation of a passenger vessel. *Math. Model. Civ. Eng.* **2010**, *2*, 17–26.
24. Caprace, J.-D.; Bair, F.; Rigo, P. Multi-criterion Scantling Optimisation of Passenger Ships. In Proceedings of the COMPIT'10-9th International Conference on Computer Applications and Information Technology in the Maritime Industries, Gubbio, Italy, 12–14 April 2010.
25. Alhammadi, H.Y.; Romagnoli, J.A. Incorporating environmental, profitability, heat integration and controllability considerations. *Integr. Process Des. Control* **2004**, *17*, 264.
26. Selvi, S.T.; Baskar, S.; Rajasekar, S. Application of evolutionary algorithm for multiobjective transformer design optimization. In *Classical and Recent Aspects of Power System Optimization*; Elsevier: Amsterdam, The Netherlands, 2018; pp. 463–504.
27. De Buck, V.; López, C.A.M.; Nimmegeers, P.; Hashem, I.; Van Impe, J. Multi-objective optimisation of chemical processes via improved genetic algorithms: A novel trade-off and termination criterion. In *Computer Aided Chemical Engineering*; Elsevier: Amsterdam, The Netherlands, 2019; pp. 613–618.
28. Wang, L.; Ng, A.H.; Deb, K. *Multi-Objective Evolutionary Optimisation for Product Design and Manufacturing*; Springer: Berlin/Heidelberg, Germany, 2011.
29. Ghanta, S.; Rayguru, M.M.; Pathmakumar, T.; Kalimuthu, M.; Elara, M.R.; Sheu, B.J. Uniform hydro blasting for ship hull maintenance: A multi-objective optimization framework. *Ocean. Eng.* **2021**, *242*, 109977. [CrossRef]
30. Leal, M.; Gordo, J.M. Hull's manufacturing cost structure. *Brodogr. Teor. I Praksa Brodogr. I Pomor. Teh.* **2017**, *68*, 1–24. [CrossRef]
31. Rigo, P.; Caprace, J.-D. Optimisation of ship structures. *Mar. Technol. Eng.* **2011**, 925–944.

32. Esmailian, E.; Steen, S. A new method for optimal ship design in real sea states using the ship power profile. *Ocean. Eng.* **2022**, *259*, 111893. [CrossRef]
33. Chowdhury, M. On the probability of failure by yielding of hull girder midship section. *Ships Offshore Struct.* **2007**, *2*, 241–260. [CrossRef]
34. Soleimani, E.; Tabeshpour, M.R.; Seif, M.S. Parametric study of buckling and post-buckling behavior for an aluminum hull structure of a high-aspect-ratio twin hull vessel. *Proc. Inst. Mech. Eng. Part M J. Eng. Marit. Environ.* **2020**, *234*, 15–25. [CrossRef]
35. Faqih, I.; Adiputra, R.; Prabowo, A.R.; Muhayat, N.; Ehlers, S.; Braun, M. Hull girder ultimate strength of bulk carrier (HGUS-BC) evaluation: Structural performances subjected to true inclination conditions of stiffened panel members. *Results Eng.* **2023**, *18*, 101076. [CrossRef]
36. Li, S.; Hu, Z.; Benson, S. A cyclic progressive collapse method to predict the bending response of a ship hull girder. In *Trends in the Analysis and Design of Marine Structures*; CRC Press: Boca Raton, FL, USA, 2019; pp. 149–157.
37. Hørte, T.; Wang, G.; White, N. Calibration of the hull girder ultimate capacity criterion for double hull tankers. In Proceedings of the PRADS 2007 Conference, Houston, TX, USA, 1–5 October 2007.